# Single-Phase Frequency-Locked Loops: A Comprehensive Review

Saeed Golestan, *Senior Member, IEEE*, Josep M. Guerrero, *Fellow, IEEE*, Fariborz Musavi, *Senior Member, IEEE*, and Juan C. Vasquez, *Senior Member, IEEE*

***Abstract*—Synchronization techniques can be classified into open-loop and closed-loop methods. In power and energy applications, which are the focus here, the latter type is more popular. Phase-locked loops (PLLs) and frequency-locked loops (FLLs) are two broad categories of closed-loop synchronization techniques. The aim of this paper is providing a review of recent advances in designing single-phase FLLs, which can be very useful for both researchers and engineers. The historical development of a standard single-phase FLL, its modeling and tuning aspects, its relationship with adaptive notch filters, its advanced versions for the synchronization purposes under adverse grid conditions, its modification for different industrial applications, its connection with single-phase PLLs, and its discretization aspects are the main parts of this review.**

***Index Terms*—Adaptive notch filters (ANFs), frequency-locked loop (FLL), phase detection, phase-locked loop (PLL), second-order generalized integrator (SOGI), synchronization.**

## I. Introduction

SYNCHRONIZATION techniques, which are highly important for different signal processing/monitoring/control purposes in energy and power applications, can be classified into two general categories: open-loop techniques [1], [2], which are characterized by having no feedback signal in their structures, and closed-loop ones [3]–[7], which have at least one feedback signal in their structures. Closed-loop synchronization (CLS) techniques have received more attention than open-loop ones.

Phase-locked loops (PLLs) [3]–[5] and frequency-locked loops (FLLs) [6], [7] are two broad categories of CLS techniques. They are both nonlinear control systems, but they are implemented in different reference frames. To be more exact, PLLs are implemented in the synchronous reference frame, and FLLs are realized in the stationary reference frame. Admittedly, FLLs are not as popular as PLLs in power applications. How-

Manuscript received September 19, 2018; revised December 30, 2018; accepted February 13, 2019. Date of publication April 10, 2019; date of current version September 6, 2019. Recommended for publication by Associate Editor L. Peng. *(Corresponding author: Saeed Golestan.)*

S. Golestan, J. M. Guerrero, and J. C. Vasquez are with the Department of Energy Technology, Aalborg University DK-9220 Aalborg, Denmark (e-mail:

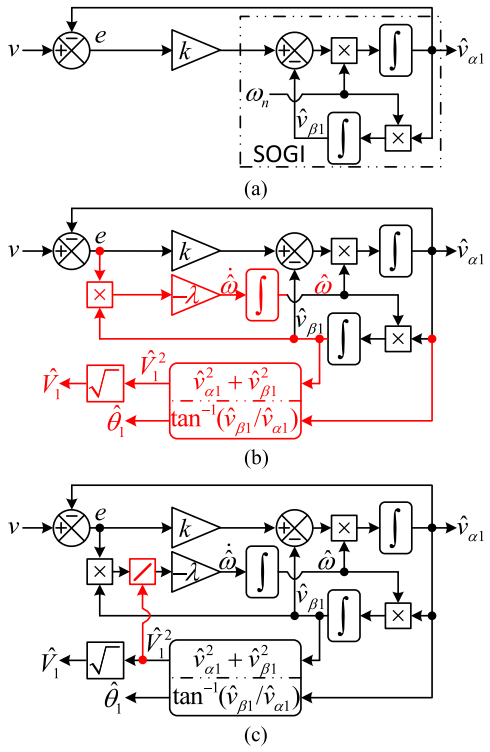


Fig. 1. Development of SOGI-FLL. (a) SOGI-QSG. (b) Adding a frequency estimator and amplitude/phase calculation parts. (c) Adding the amplitude normalization part. $v$ is the single-phase input signal; $\hat{v}_{\alpha_1}$ and $\hat{v}_{\beta_1}$ are estimations of the fundamental component of the input signal and its quadrature version, respectively; and $\hat{\theta}_1$, $\hat{V}_1$, and $\hat{\omega}$ denote an estimation of the phase, amplitude, and angular frequency of the input signal, respectively. $\omega_n$ denotes the nominal angular frequency of the input signal, $k$ is the SOGI-QSG gain, and $\lambda$ is the frequency estimator gain.

and (2) express the SOGI-QSG characteristic transfer functions and Fig. 2 illustrates their Bode plots

$$G_\alpha(s)=\frac{\hat{v}_{\alpha 1}(s)}{v(s)}=\frac{k\omega_n s}{s^2+k\omega_n s+\omega_n^2} \tag{1}$$

$$G_\beta(s)=\frac{\hat{v}_{\beta 1}(s)}{v(s)}=\frac{k\omega_n^2}{s^2+k\omega_n s+\omega_n^2}. \tag{2}$$

Notice that the transfer functions (1) and (2) act as a band-pass filter (BPF) with the center frequency at $\omega_n$ and a low-pass filter (LPF) with a 0-dB gain and $-90^\circ$ phase at $\omega_n$, respectively. Therefore, as long as the input signal frequency is fixed or very close to its nominal value, the $\alpha$- and $\beta$-axis outputs of the SOGI-QSG provide an accurate estimation of the input signal fundamental component and its quadrature version, respectively. However, in power and energy applications, which are the focus here, the aforementioned condition for the input signal frequency may not always exist. This is particularly true for microgrids and weak grid conditions. Therefore, designing an estimator for extracting the input signal frequency and adapting the SOGI center frequency to frequency changes is necessary.

Such an estimator can be designed using the gradient descent method [5], [26], [27]. To this end, the input and output signals

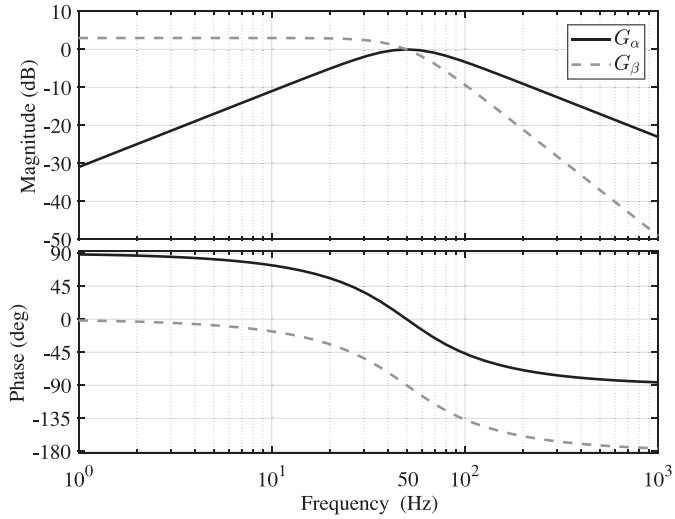


Fig. 2. Bode plots of transfer functions $G_\alpha(s)$ and $G_\beta(s)$, which are expressed in (1) and (2), respectively. Parameters: $\omega_n=2\pi 50$ rad/s and $k=\sqrt{2}$.

of the SOGI-QSG are first considered as

$$v=V_1\cos(\theta_1) \tag{3}$$

$$\hat{v}_{\alpha 1}=\hat{V}_1\cos(\hat{\theta}_1) \tag{4}$$

$$\hat{v}_{\beta 1}=\hat{V}_1\sin(\hat{\theta}_1) \tag{5}$$

where $V_1$ and $\theta_1=\int_0^t\omega d\tau+\varphi_1$ are the amplitude and phase angle of the input signal of the SOGI-QSG, respectively, $\omega$ and $\varphi_1$ denote the angular frequency and initial phase angle, respectively, and $\hat{}$ refers to estimated quantities. Then, the cost function (6) is defined, and the gradient descent method is applied to direct the frequency of the output signal toward the input one. Equation (7) describes the differential equation of the obtained frequency estimator, in which $\lambda$ is a control parameter that determines the speed of convergence

$$J=\frac{1}{2}e^2=\frac{1}{2}[v-\hat{v}_{\alpha 1}]^2=\frac{1}{2}[V_1\cos(\theta_1)-\hat{V}_1\cos(\hat{\theta}_1)]^2 \tag{6}$$

$$\dot{\hat{\omega}}=-\lambda\frac{\delta J}{\delta\hat{\omega}}=-\lambda\underbrace{\frac{\delta J}{\delta e}}_{e}\underbrace{\frac{\delta e}{\delta\hat{\theta}_1}}_{\hat{v}_{\beta 1}}\underbrace{\frac{\delta\hat{\theta}_1}{\delta\hat{\omega}}}_{t}=-\lambda te\hat{v}_{\beta 1}. \tag{7}$$

As shown in (7), the time variable $t$ appears in the frequency estimator differential equation. This makes the frequency estimator unstable. To deal with this problem, the time variable $t$ can be simply ignored [27], which results in

$$\dot{\hat{\omega}}=-\lambda e\hat{v}_{\beta 1}. \tag{8}$$

Notice that neglecting $t$ is intuitively reasonable because it is always positive. More details about this issue can be found in [27].

Adding the frequency estimator (8) to the SOGI-QSG structure results in Fig. 1(b) [6], [9]. Thanks to this estimator, which adapts the SOGI center frequency to frequency changes, the input signal fundamental component and its quadrature ver-

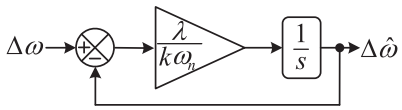


Fig. 3. First-order LTI model of the SOGI-FLL [6].

sion can now be accurately extracted under both nominal and off-nominal frequencies. Using these signals, the phase and amplitude of the input signal may also be easily calculated (if required) as $\hat{\theta}_1 = \tan^{-1}(\hat{v}_{\beta 1}/\hat{v}_{\alpha 1})$ and $\hat{V}_1 = \sqrt{\hat{v}_{\alpha 1}^2 + \hat{v}_{\beta 1}^2}$, as highlighted in Fig. 1(b).

By substituting (3)–(5) into (8), it can be rewritten as

$$\dot{\hat{\omega}} = -\lambda \hat{V}_1 \sin(\hat{\theta}_1)\left[V_1 \cos(\theta_1) - \hat{V}_1 \cos(\hat{\theta}_1)\right]$$

$$= \frac{\lambda \hat{V}_1}{2}\left[V_1 \sin(\theta_1 - \hat{\theta}_1) - \boldsymbol{V_1 \sin(\theta_1 + \hat{\theta}_1)} + \boldsymbol{\hat{V}_1 \sin(2\hat{\theta}_1)}\right]. \tag{9}$$

Neglecting the double-frequency (highlighted) terms in (9) gives

$$\dot{\hat{\omega}} \approx \frac{\lambda \boldsymbol{V_1 \hat{V}_1}}{2} \sin(\theta_1 - \hat{\theta}_1). \tag{10}$$

From (10), it can be observed that the frequency estimator dynamics depend on the input signal amplitude. It implies that any change in this parameter may affect the performance of this estimator. Therefore, to decouple the frequency estimator dynamics from input signal amplitude changes, an amplitude normalization stage, as highlighted in Fig. 1(c), may also be included into the frequency estimator [6]. This final product [see Fig. 1(c)] is called the SOGI-FLL. Notice that, to avoid division by zero during the start-up and transients, a saturation needs to be included before the division operation.

It has to be mentioned here that in the original structure of the SOGI-FLL (see [6, Fig. 6] or [9, Fig. 8]), in addition to the aforementioned amplitude normalization, the estimated frequency $\hat{\omega}$ is fed back and multiplied by the frequency estimator gain. This feedback signal is supposedly intended to make the frequency estimator dynamics independent of the input signal frequency. However, the frequency estimator differential equation (10), which can be rewritten as (11) by considering the aforementioned amplitude normalization, does not indicate any direct dependence on the input signal frequency. Indeed, it is approximately proportional to the phase error signal. Considering this fact, it can be concluded that the aforementioned frequency feedback is unnecessary and, therefore, is not considered throughout this paper

$$\dot{\hat{\omega}} \approx \frac{\lambda}{2} \sin(\theta_1 - \hat{\theta}_1) \approx \frac{\lambda}{2}(\theta_1 - \hat{\theta}_1). \tag{11}$$

### *B. Modeling*

The first attempt to obtain a linear model for the SOGI-FLL has been made in [6]. In this work, a first-order linear time-invariant (LTI) model, as expressed in (12) and as shown in Fig. 3, is presented for describing the frequency estimation dynamics of the SOGI-FLL

$$\Delta\hat{\omega}(s) \approx \frac{\lambda/(k\omega_n)}{s + \lambda/(k\omega_n)} \Delta\omega(s). \tag{12}$$

Notice that the input signal amplitude does not appear in this differential equation because of the amplitude normalization in the SOGI-FLL structure.

This model has two main limitations: 1) it does not predict the SOGI-FLL dynamics in estimating the phase and amplitude; and 2) it cannot accurately predict the SOGI-FLL frequency estimation dynamics in all scenarios, particularly when the SOGI-FLL has a low damping factor. To deal with these limitations, more accurate and complete modeling of the SOGI-FLL is presented in [7] and [11]. This modeling method is briefly explained in what follows.

According to Fig. 1(c), the estimated phase and amplitude can be expressed as

$$\hat{\theta}_1 = \tan^{-1}\left(\frac{\hat{v}_{\beta 1}}{\hat{v}_{\alpha 1}}\right) \tag{13}$$

$$\hat{V}_1 = \sqrt{\hat{v}_{\alpha 1}^2 + \hat{v}_{\beta 1}^2}. \tag{14}$$

Differentiating (13) and (14) with respect to time gives

$$\dot{\hat{\theta}}_1 = \frac{\dot{\hat{v}}_{\beta 1}\hat{v}_{\alpha 1} - \dot{\hat{v}}_{\alpha 1}\hat{v}_{\beta 1}}{\hat{V}_1^2} \tag{15}$$

$$\dot{\hat{V}}_1 = \frac{\hat{v}_{\alpha 1}\dot{\hat{v}}_{\alpha 1} + \hat{v}_{\beta 1}\dot{\hat{v}}_{\beta 1}}{\hat{V}_1} \tag{16}$$

where $\dot{\hat{v}}_{\alpha 1}$ and $\dot{\hat{v}}_{\beta 1}$, according to Fig. 1(c), are equal to

$$\dot{\hat{v}}_{\alpha 1} = \hat{\omega}\left(-\hat{v}_{\beta 1} + kv - k\hat{v}_{\alpha 1}\right) \tag{17}$$

$$\dot{\hat{v}}_{\beta 1} = \hat{\omega}\hat{v}_{\alpha 1}. \tag{18}$$

Substituting (17) and (18) into (15) and (16) and considering the definitions (3)–(5) gives

$$\dot{\hat{\theta}}_1 = \hat{\omega} + \frac{k}{\lambda}\hat{\omega}\dot{\hat{\omega}} \tag{19}$$

$$\dot{\hat{V}}_1 = \frac{k\hat{\omega}(v - \hat{v}_{\alpha 1})\hat{v}_{\alpha 1}}{\hat{V}_1}$$

$$= \frac{k\hat{\omega}}{2}\left[V_1 \cos(\theta_1 - \hat{\theta}_1) - \hat{V}_1 + \boldsymbol{V_1 \cos(\theta_1 + \hat{\theta}_1)} - \boldsymbol{\hat{V}_1 \cos(2\hat{\theta}_1)}\right]. \tag{20}$$

By assuming a quasi-locked state, i.e., $\hat{V}_1 \approx V_1$, $\hat{\omega} \approx \omega$, and $\hat{\theta}_1 \approx \theta_1$, and defining $\hat{V}_1 = V_n + \Delta\hat{V}_1$, $V_1 = V_n + \Delta V_1$, $\hat{\omega} = \omega_n + \Delta\hat{\omega}$, $\omega = \omega_n + \Delta\omega$, $\hat{\theta}_1 = \theta_n + \Delta\hat{\theta}_1$, $\theta_1 = \theta_n + \Delta\theta_1$, where the subscript $n$ denotes the nominal value and $\Delta$ denotes a small perturbation, (19) and (20) can be approximated by

$$\Delta\dot{\hat{\theta}}_1 \approx \Delta\hat{\omega} + \frac{k\omega_n}{\lambda}\Delta\dot{\hat{\omega}} \tag{21}$$

$$\Delta\dot{\hat{V}}_1 \approx \frac{k\omega_n}{2}(\Delta V_1 - \Delta\hat{V}_1). \tag{22}$$

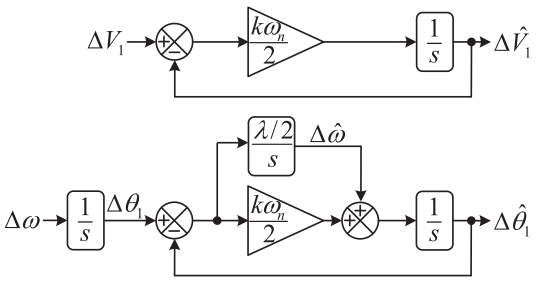


Fig. 4. Second-order LTI model of the SOGI-FLL [7], [11].

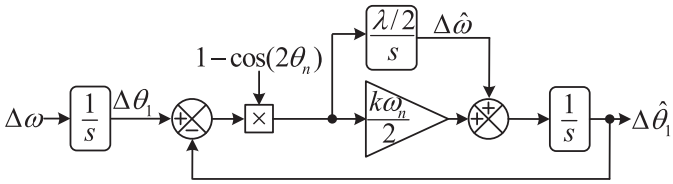


Fig. 5. LTP model of the SOGI-FLL [28].

Using (11) and considering the definitions made before for $\theta_1$ and $\hat{\theta}_1$, the SOGI-FLL frequency estimator dynamics may also be linearized as follows:

$$\Delta\dot{\hat{\omega}} \approx \frac{\lambda}{2}(\Delta\theta_1 - \Delta\hat{\theta}_1). \tag{23}$$

Based on (21)–(23), the SOGI-FLL linear model can be obtained, as illustrated in Fig. 4. Notice that this model is a second-order LTI model.

During transients, the SOGI-FLL demonstrates some damped double-frequency oscillations in its estimated parameters. The highlighted terms in (9) and (20) formulate these oscillations. During the aforementioned modeling procedure, which is a rather short version of the modeling method presented in [7] and [11], these double-frequency oscillations were neglected. It implies that the second-order LTI model (see Fig. 4) cannot predict these oscillations in the SOGI-FLL transient response. In [28], a more accurate modeling procedure for single-phase grid synchronization techniques (including the SOGI-FLL) is presented, which takes into account these oscillations. This method results in a linear-time periodic (LTP) model, as shown in Fig. 5.[1] Notice that the only difference between this model and the second-order LTI one is the excitation by a double-frequency trigonometric term.

To gain insight about the accuracy of the available models for the SOGI-FLL (i.e., Figs. 3–5), a comparison among them in predicting the SOGI-FLL transient behavior in response to a +2-Hz frequency jump is carried out. The results of this comparison can be seen in Fig. 6. Based on these results, the following observations can be made.

[1]During the LTP modeling of the SOGI-FLL in [28], for the sake of brevity, only the phase and frequency estimation dynamics are linearized and modeled. An LTP model for the SOGI-FLL amplitude estimation dynamics may also be easily obtained by following a similar procedure.

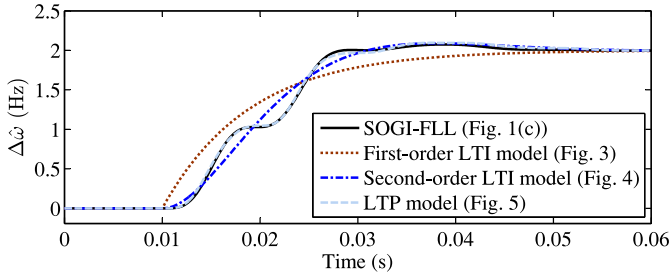


Fig. 6. Accuracy assessment of the available models for the SOGI-FLL in response to +2-Hz frequency jump. In the case of the SOGI-FLL [see Fig. 1(c)], the signal $\Delta\hat{\omega}$ may be obtained by subtracting $\omega_n = 2\pi 50$ rad/s from the estimated frequency $\hat{\omega}$. The control parameters are [11]: $k = \sqrt{2}$ and $\lambda = 49348$. In all numerical results in this paper (unless otherwise stated), the sampling frequency is 10 kHz, and the input signal amplitude is 1 per unit (p.u.)

1) The LTP model (see Fig. 5) yields a remarkable accuracy as it can even predict the damped double-frequency oscillations in the SOGI-FLL transient behavior.
2) The second-order LTI model (see Fig. 4) predicts the average dynamic behavior of the SOGI-FLL accurately. However, it cannot predict the double-frequency oscillations.
3) The first-order LTI model (see Fig. 3) gives a rather poor accuracy, as it cannot precisely predict the average dynamic behavior of the SOGI-FLL.

Based on these observations, using the first-order LTI model (see Fig. 3) for the SOGI-FLL dynamic assessment and tuning is not recommended. The second-order LTI model (see Fig. 4) is indeed the most suitable option for these purposes, as it is accurate enough in most practical scenarios, and at the same time, the concept of the transfer function is applicable to it. Notice that, in the case of the SOGI-FLL LTP model (see Fig. 5), or generally all LTP systems, the transfer function representation is ambiguous because there is a coupling among different frequencies in their input and output [28]. To deal with this problem, a more general concept, called the harmonic transfer function, has been introduced, which translates the LTP system into a doubly infinite LTI one [29]. It, however, demands using multi-input multi-output control methods for the analysis, which is a bit complicated. Despite this fact, the great accuracy of the LTP model is still a valuable asset and can be useful for stability studies [28]. This is particularly true under weak grid conditions, where interactions between the grid-tied power converter and its synchronization unit cause serious stability concerns [30].

### C. Tuning Control Parameters

From Fig. 4, the key transfer functions of the SOGI-FLL can be obtained as

$$G_{cl}^{V}(s) = \frac{\Delta\hat{V}_1(s)}{\Delta V_1(s)} = \frac{k\omega_n/2}{s + k\omega_n/2} \tag{24}$$

$$G_{cl}^{\omega}(s) = \frac{\Delta\hat{\omega}(s)}{\Delta\omega(s)} = \frac{\lambda/2}{s^2 + (k\omega_n/2)\,s + \lambda/2} \tag{25}$$

$$G_{cl}^{\theta}(s) = \frac{\Delta\hat{\theta}_1(s)}{\Delta\theta_1(s)} = \frac{(k\omega_n/2)\,s + \lambda/2}{s^2 + (k\omega_n/2)\,s + \lambda/2}. \tag{26}$$

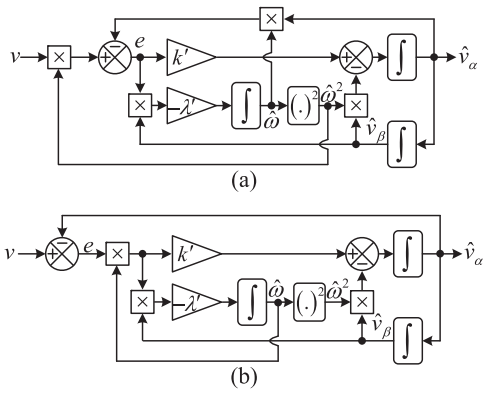


Fig. 7. Block diagrams of two ANFs. (a) ANF1 [34]. (b) ANF2 [18]. In both structures, $k'$ and $\lambda'$ are the generalized integrator (GI) and frequency estimator gains, respectively. $\hat{v}_\alpha$ and $\hat{v}_\beta$ are signals with the same phase and 90° phase delay compared to the input signal fundamental component, respectively.

Using these transfer functions and the characteristic transfer functions of the SOGI-QSG [i.e., (1) and (2)], the SOGI-FLL tuning procedure can be easily carried out. A possible tuning method is briefly presented in what follows.

Using (1) and (2), it can be demonstrated that an optimal tradeoff between the setting time and overshoot in the extraction of the fundamental component and its quadrature version is obtained if $k = \sqrt{2}$ is selected. That is the reason why this value is often recommended as a good choice in the literature [6], [11]. This selection, however, may not be able to provide a high filtering capability. Consequently, if a higher disturbance rejection ability is desired, one can select a lower value for this parameter, but at the cost of a slower transient response.

The characteristic polynomial of both transfer functions (25) and (26) is

$$s^2 + \underbrace{(k\omega_n/2)}_{2\zeta\omega_n'} s + \underbrace{\lambda/2}_{(\omega_n')^2} = 0 \tag{27}$$

in which $\zeta$ and $\omega_n'$ are the damping factor and the natural frequency, respectively. By selecting $\zeta = 1/\sqrt{2}$, which is often recommended as the optimum damping factor in the literature, $\lambda$ can be expressed as

$$\lambda = 2(\omega_n')^2 = \frac{k^2\omega_n^2}{4}. \tag{28}$$

Substituting the recommended value for $k$, i.e., $k = \sqrt{2}$, into (28) gives $\lambda = \omega_n^2/2 = 49348$.

## III. ANFs: Close Variants of the SOGI-FLL

The development of an ANF dates back to around three decades ago when it was first designed and proposed by Regalia as a lattice filter structure in the discrete-time domain [31]. After several years, Bodson and Douglas [32] proposed a continuous-time version of this structure, which was later modified by Hsu *et al.* [33]. To simplify the tuning procedure for Hsu's ANF and make its periodic orbit independent of its control parameters, a simple modification was suggested in [34]. Fig. 7(a) illustrates the resultant structure, which is called here the ANF1.

TABLE I
Fair Condition of Comparison Among SOGI-FLL and ANFs

| | GI gain | Frequency estimator gain |
|---|---|---|
| SOGI-FLL | $k$ | $\lambda$ |
| ANF1 | $k' = k$ | $\lambda' = \lambda/w_n^2$ |
| ANF2 | $k' = k$ | $\lambda' = \lambda$ |

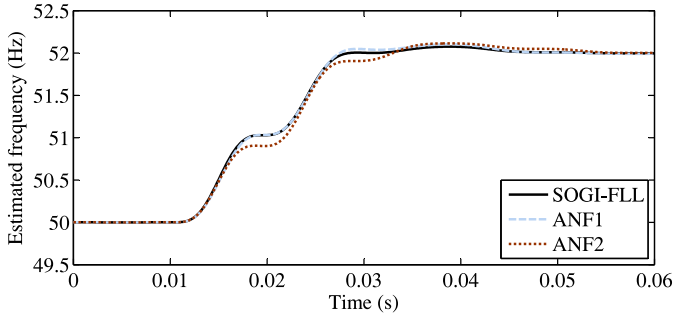


Fig. 8. Performance comparison between the SOGI-FLL and ANFs shown in Fig. 7 in response to a +2-Hz frequency jump. The SOGI-FLL control values are $k = \sqrt{2}$ and $\lambda = 49\,348$ [11]. Control parameters of the ANFs can be calculated according to Table I. The grid voltage amplitude is fixed at 1 p.u.

If we assume that the input signal of the ANF1 is as (3), then its $\alpha$-axis output will be equal to $\hat{v}_\alpha(t) = \hat{\omega}\hat{V}_1\cos(\hat{\theta}_1)$. It implies that the $\alpha$-axis output should be divided by $\hat{\omega}$ to give an estimation of the input signal fundamental component. To eliminate the need for such a division and directly obtain the input signal fundamental component, restructuring the ANF1, as shown in Fig. 7(b), is suggested in [18]. This structure is called here the ANF2.

These ANFs have a very close relationship with the standard SOGI-FLL. This fact has already been pointed out in some publications [35], [36]. It, however, does not seem to be widely known by researchers. An example to support this claim is [10], in which totally different results for the SOGI-FLL and an ANF have been reported (see [10, Table I]). These results are because of considering an unfair condition of comparison between the SOGI-FLL and the ANF.

The close relationship of the SOGI-FLL and ANFs can be demonstrated theoretically or numerically. Here, to better visualize it, the numerical way is considered. Table I summarizes the fair condition of comparison among the SOGI-FLL and ANFs. A way of finding this condition is deriving small-signal models of the ANFs by following a similar procedure as that explained for the SOGI-FLL (see Section II-B).

Fig. 8 illustrates the obtained results in response to a +2-Hz frequency jump. It can be observed that the SOGI-FLL and ANFs demonstrate a close performance.[2] This fact can be further supported by using other tests,[3] which are not presented here to save space.

[2]To preserve this relationship under voltage sags/swells, using an amplitude normalization in the ANFs is required.

[3]The dynamic performance difference between the SOGI-FLL and ANFs may become more noticeable under a severe phase jump, as it results in large transients in the estimated frequency.

At the end of this section, it may be interesting to briefly discuss why the structures shown in Fig. 7 are called an ANF at all. The key to answering this question is obtaining transfer functions relating the error signal $e$ to the input signal $v$ in these structures. Assuming that the estimated frequency $\hat{\omega}$ is a constant, these transfer functions can be expressed as

$$\text{ANF1} \quad \Rightarrow \quad \frac{e(s)}{v(s)} = \frac{\hat{\omega}^2(s^2+\hat{\omega}^2)}{s^2+k'\hat{\omega}s+\hat{\omega}^2} \tag{29}$$

$$\text{ANF2} \quad \Rightarrow \quad \frac{e(s)}{v(s)} = \frac{(s^2+\hat{\omega}^2)}{s^2+k'\hat{\omega}s+\hat{\omega}^2}. \tag{30}$$

Both these transfer functions describe a notch filter (NF) with the notch frequency at $\hat{\omega}$. As this notch frequency is adaptive in practice, they are called an ANF.

## IV. Advanced SOGI-FLLs for the Grid Synchronization

This section provides an overview of some recently designed advanced single-phase FLLs for grid synchronization purposes. What almost all these FLLs have in common is using the standard SOGI-FLL structure as the basic building block. Improving the standard SOGI-FLL performance, particularly its filtering capability, is the main objective in designing these FLLs.

### A. SOGI-FLL With DC Rejection Capability (SOGI-FLL-WDCRC)

For many reasons, in addition to the fundamental component, a dc component may also appear in the SOGI-FLL input. For example, in grid-connected applications, short circuits and faults, saturation of current transformers, geomagnetic storms, half-wave rectification, and dc injection by distributed generation systems may cause a dc component in the grid voltage and, therefore, in the SOGI-FLL input [36], [37]. The data conversion process is another reason that may cause a dc offset [38]. In what follows, the performance of the standard SOGI-FLL in the presence of a dc component in its input is briefly examined, and an available standard method to deal with this problem is explained.

From (1), it can be observed that the transfer function $G_\alpha(s)$, which relates the $\alpha$-axis output of the SOGI-QSG to its input, has a zero dc gain. It means that the $\alpha$-axis output is free from any dc component in the presence of such a component in the SOGI-QSG input. The transfer function (2), however, has a dc gain equal to $k$. Therefore, if we assume that the dc offset in the SOGI-QSG input is $v_0$, a dc component equal to $kv_0$ appears in its $\beta$-axis output in the steady state. This dc component results in fundamental-frequency oscillatory errors in the estimated phase, frequency, and amplitude by the SOGI-FLL.

To reject the dc component disturbance effect on the SOGI-FLL performance and, at the same time, to provide an estimation of this component, modifying the SOGI-FLL structure based on the gradient descent method has been suggested in [36]. This method is briefly introduced here.

Assume that the SOGI-FLL input signal is as follows:

$$v = V_1\cos(\theta_1) + v_0 \tag{31}$$

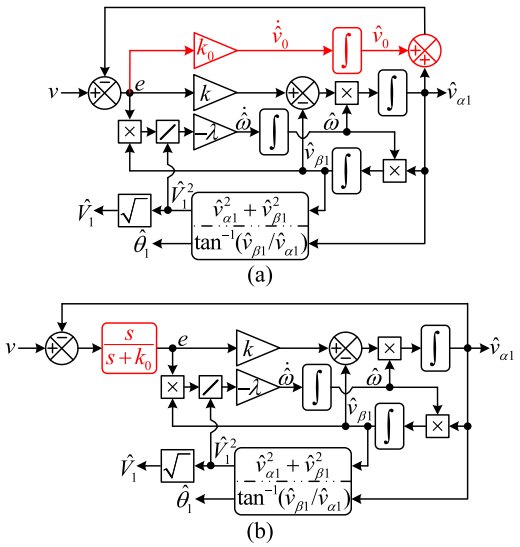


Fig. 9. (a) Block diagram of the SOGI-FLL-WDCRC [36]. (b) Its alternative representation.

where $v_0$, as mentioned before, denotes the dc component. Also, assume that $\hat{v}_0$ is an estimation of this component, which is supposed to be provided by adding a control loop to the standard SOGI-FLL. Based on these assumptions, the following cost function can be defined:

$$J = \frac{1}{2}e^2 = \frac{1}{2}(v-\hat{v}_{\alpha 1}-\hat{v}_0)^2 = \frac{1}{2}\Big(V_1\cos(\theta_1)+v_0-\hat{V}_1\cos(\hat{\theta}_1)-\hat{v}_0\Big)^2. \tag{32}$$

Applying the gradient descent method to (32) gives the update law for $\hat{v}_0$ as

$$\dot{\hat{v}}_0 = -k_0\frac{\delta J}{\delta \hat{v}_0} = -k_0\underbrace{\frac{\delta J}{\delta e}}_{e}\underbrace{\frac{\delta e}{\delta \hat{v}_0}}_{-1} = k_0 e. \tag{33}$$

In (33), $k_0$ is a design constant, which adjusts the speed of the dc-offset estimation. Based on (33), a dc-offset estimation/rejection loop can be added to the standard SOGI-FLL, as highlighted in Fig. 9(a) [36]. A similar structure to Fig. 9(a) may also be found in [39]. Some guidelines for tuning the control parameters of this structure have been suggested in [36]. No small-signal model for this structure has yet been presented.

It is worth mentioning here that adding the dc estimation/rejection loop to the SOGI-FLL is mathematically equivalent to including a first-order high-pass filter into its control loop, as shown in Fig. 9(b).

### B. Multiple-SOGI-Based FLL (MSOGI-FLL)

Harmonics are those disturbances that their frequencies are integer multiples of the fundamental frequency. They are often caused by nonlinear loads and may adversely affect the SOGI-FLL performance by causing oscillatory ripples in its estimated parameters.

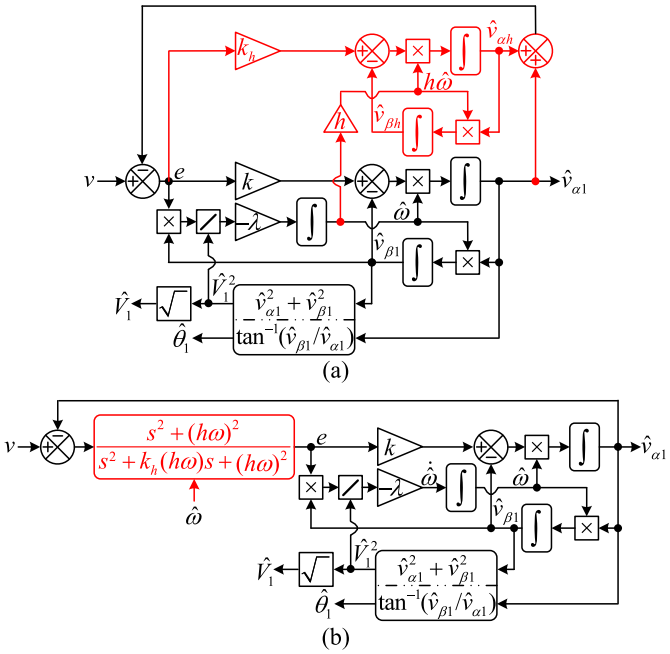


Fig. 10. (a) SOGI-FLL with one harmonic rejection/estimation ability [6]. (b) Its alternative representation. $h$ denotes the order of the concerned harmonic component.

The structure of the standard SOGI-FLL can be extended to take into account the presence of one or more harmonic components. To this end, one or more SOGIs centered at the concerned harmonic frequencies are connected in parallel with the main SOGI, which result in an MSOGI-FLL [6]. The center frequencies of these SOGIs are adapted to grid frequency changes using the estimated frequency. Fig. 10(a) illustrates the resultant structure for the simplest possible case, i.e., when rejecting/estimating one harmonic component is required. Notice that, as highlighted in Fig. 10(b), this harmonic estimation/rejection loop is mathematically equivalent to including an adaptive second-order NF with the notch frequency at the concerned harmonic frequency in the SOGI-FLL control loop. No small-signal model for the MSOGI-FLL has yet been presented.

### C. SOGI-FLL With Prefilter (SOGI-FLL-WPF)

In practice, the SOGI-FLL input signal may contain a large number of harmonics. In this case, removing all these disturbances by using parallel SOGIs, as described in Section IV-B, may not be very practical from the computational point of view. To deal with this challenge, adding one or more adaptive BPFs before the SOGI-FLL input is suggested in [40]. Fig. 11 illustrates the simplest possible case of this idea, in which only one adaptive BPF is employed as the prefilter. This structure is called the SOGI-FLL-WPF. Notice that the BPF (the prefilter) in this structure is actually a SOGI-QSG, whose $\alpha$-axis output is only used. The center frequency of this BPF is adapted to frequency changes using a frequency feedback loop. Notice also that the BPF completely rejects the dc offset and, depending on its bandwidth, may considerably attenuate harmonics and interharmonics.

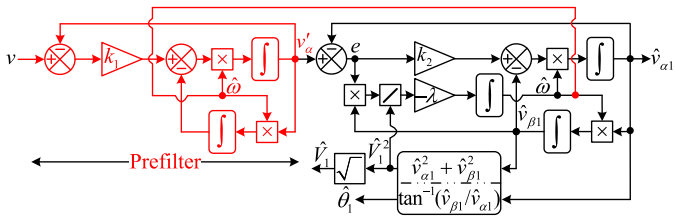


Fig. 11. SOGI-FLL-WPF [40].

In [7], a small-signal model[4] for the SOGI-FLL-WPF is derived, and a systematic method for tuning its control parameters is presented. This model can be easily extended to the case where more than one SOGI-based BPF are used as the prefilter.

### D. Fourth-Order Generalized Integrator-Based FLL (FOGI-FLL)

In [35] and [41], a different FLL called the FOGI-FLL is presented. The procedure for developing this FLL can be observed in Fig. 12. It is discussed in [41] that replacing the loop integrator of a first-order LPF [see Fig. 12(a)] by a SOGI results in the SOGI-QSG [see Fig. 12(b)]. Based on this fact, developing a fourth-order generalized integrator-based QSG (FOGI-QSG), as shown in Fig. 12(d), through replacing two integrators of a second-order LPF [see Fig. 12(c)] by two SOGIs is suggested in [41]. It is demonstrated in [41] that the FOGI-QSG completely rejects the dc component and provides a higher harmonic/interharmonic rejection capability than the SOGI-QSG. This fact may also be verified by obtaining the transfer functions relating the $\alpha\beta$-axis outputs of the FOGI-QSG to its input signal. The FOGI-FLL, as illustrated in Fig. 12(e), is finally developed by adding the same frequency estimator as that of the standard SOGI-FLL to the FOGI-QSG [35].

By modifying the FOGI-FLL structure, it can be restructured, as shown in Fig. 12(f), in which $k_1 = k$, $k_2 = k'$, and $\lambda = k'\lambda'/k$. This structure is called the SOGI-FLL with in-loop filter (SOGI-FLL-WIF) [7]. The equivalence of the FOGI-FLL and SOGI-FLL-WIF can be easily verified using numerical tests. This representation of the FOGI-FLL [see Fig. 12(f)] demonstrates that it is actually a standard SOGI-FLL, where an adaptive SOGI-based BPF has been included in its control loop.

In [7], a small-signal model[5] for the SOGI-FLL-WIF [see Fig. 12(f)] is presented, and a systematic approach based on the symmetrical optimum method for tuning its control parameters is suggested. A performance comparison between the standard SOGI-FLL, SOGI-FLL-WPF, and SOGI-FLL-WIF under a fair condition is also conducted to highlight their advantages and disadvantages. It is demonstrated that the SOGI-FLL-WPF and SOGI-FLL-WIF have a close performance and stability margin [7]. It is also shown that these two advanced FLLs offer a higher disturbance rejection capability compared to the standard SOGI-FLL, but at the cost of a lower phase margin, a larger

[4]This model is accurate as long as the SOGI-FLL-WPF has a low bandwidth.
[5]This model is accurate as long as the SOGI-FLL-WIF has a low bandwidth.

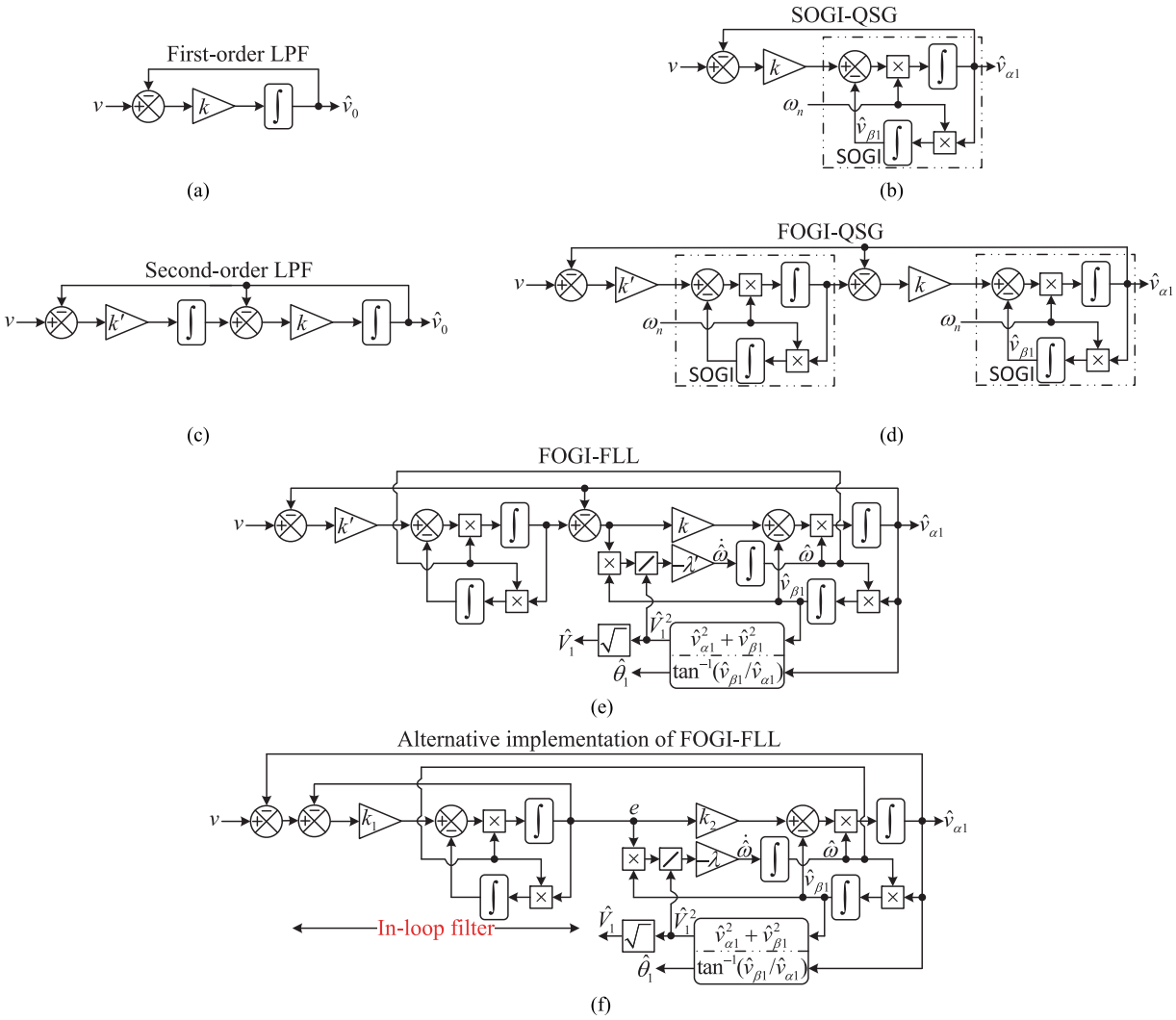


Fig. 12. Development of the FOGI-FLL. (a) First-order LPF. (b) SOGI-QSG. (c) Second-order LPF. (d) FOGI-QSG [41]. (e) FOGI-FLL [35]. (f) Alternative implementation of the FOGI-FLL, which is called the SOGI-FLL-WIF [7]. The equivalence condition between the SOGI-FLL-WIF and FOGI-FLL is: $k_1 = k$, $k_2 = k'$, and $\lambda = k'\lambda'/k$.

overshoot during transients, and a rather higher computational demand [7].

### *E. SOGI-FLL With Soft Startup (SOGI-FLL-WSS)*

In all CLS techniques, including the SOGI-FLL, there is a coupling between phase and frequency variables [42]. It implies that during the startup or under phase jumps, the estimated frequency may undergo large spurious changes [42]. Equation (11), which is the differential equation of the SOGI-FLL frequency estimator, confirms this fact. Notice that the signal $\dot{\hat{\omega}}$, which drives the frequency estimator integrator, is approximately proportional to the phase error signal $\theta_1 - \hat{\theta}_1$ when this error is small.

To enhance the SOGI-FLL dynamic performance during the startup and under phase jumps, modifying its frequency update law as expressed in (34) is suggested in [42]

$$\dot{\hat{\omega}} = -\frac{\lambda}{\hat{V}_1^2 + \boldsymbol{\gamma e^2}} e\hat{v}_{\beta 1}. \tag{34}$$

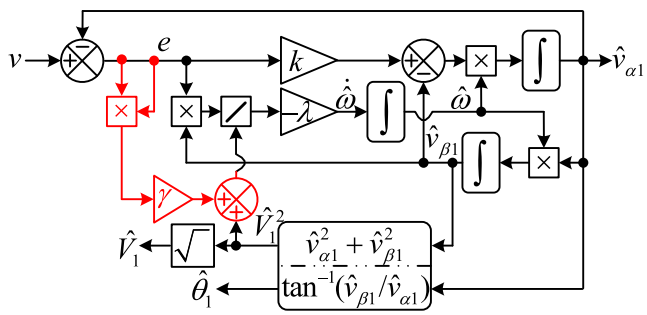

Fig. 13. SOGI-FLL-WSS [42]. $\gamma$ is a positive design constant.

This modification is highlighted in Fig. 13. In this way, during the startup and phase jumps, the frequency estimator loop gain is reduced, which prevents large spurious variations in the estimated frequency and, therefore, results in a faster and smoother transient response. This method, however, increases

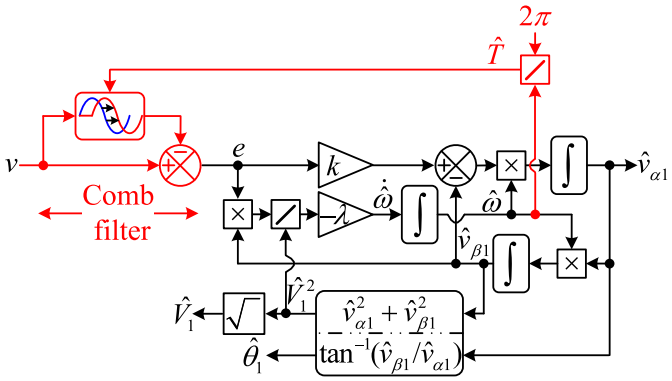


Fig. 14. Comb-FLL [45]. $\hat{T} = 2\pi/\hat{\omega}$ is an estimation of the fundamental period of the input signal. The parameter $k$ in this structure should always be equal to $1/\pi$.

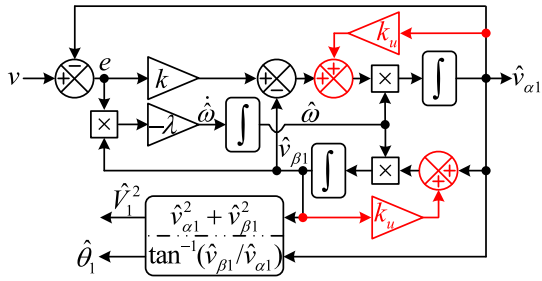


Fig. 15. Block diagram representation of the LCO-FLL [10]. $k_u = 1 - \hat{V}_1^2/A^2$, where $A$ is a constant.

the SOGI-FLL nonlinearity and, consequently, makes the small-signal modeling and stability analysis difficult. Notice that this modification has no noticeable effect on the SOGI-FLL disturbance rejection capability. Some guidelines for selecting the design constant $\gamma$ may be found in [42].

It is worth mentioning here that some other attempts to enhance the SOGI-FLL dynamic performance have been made, in which the SOGI-FLL frequency estimator gain is continuously updated using a fuzzy regulator [43], [44]. Designing these works seems to be based on a common misconception about the SOGI-FLL, i.e., considering the input signal of its frequency estimator integrator as a frequency error term. This signal, however, as shown in (11), is a phase error term.

### F. Comb-FLL

The main objective in designing the comb-FLL [45], similar to the case of the SOGI-FLL-WPF and SOGI-FLL-WIF, is improving the standard SOGI-FLL filtering capability without significantly increasing the implementation complexity and computational burden. The operating principle of this FLL is briefly explained in what follows.

As discussed before and shown in Fig. 10, adding a parallel harmonic rejection loop (a parallel SOGI) to the standard SOGI-FLL is mathematically equivalent to including a second-order ANF in its control loop. Such an NF causes two complex-conjugate zeros at the concerned harmonic frequency and, therefore, cancels the corresponding harmonic component. Based on this idea, using a comb filter, which is realized by delaying the input signal by one cycle and subtracting it from the original signal, is suggested in [45]. Fig. 14 illustrates this idea. Such a filter results in a cluster of zeros at zero, fundamental, and all harmonic frequencies up to the aliasing point and, therefore, can remove the dc component and all harmonics. Notice that the length of the delay is updated using a frequency feedback loop.

Thanks to the action of the comb filter in its input, the comb-FLL offers a high disturbance rejection capability. This advantage, however, is at the cost of a high memory requirement when the sampling frequency is high. Notice that, as mentioned before, implementing the comb-FLL involves storing one cycle of data samples in the memory. Regardless of this issue, there are some complexities, such as approximating a fractional delay and compensating an accumulated round-off error[6] in the digital implementation of the comb-FLL, which could make it less attractive for practical scenarios.[7]

### G. Limit-Cycle Oscillator-Based FLLs (LCO-FLLs)

One of the first attempts to design an LCO-FLL has been made in [10]. The main objective in designing this FLL is generating a robust synchronized signal to amplitude variations of the input signal. The block diagram representation of this FLL can be observed in Fig. 15 [10]. As shown, the LCO-FLL is realized by adding two feedback loops to the SOGI-FLL structure and removing its amplitude normalization. The gain of these feedback loops, which are highlighted in Fig. 15, is $k_u = 1 - \hat{V}_1^2/A^2$, where $A$ is a constant. According to the information given in [10], the parameter $A$ is the value at which the synchronized signals are supposed to fix their amplitude. Considering this fact, it is reasonable to consider it equal to the input signal nominal amplitude. In this condition, when the input signal amplitude is equal to its nominal value, the gain $k_u$ experiences rather small fluctuations during transients and is equal to zero in the steady state. It implies that the LCO-FLL and SOGI-FLL demonstrate a rather close performance in this condition. However, when the input signal amplitude deviates from its nominal value, the average value of $k_u$ becomes unequal to zero. Therefore, a nonorthogonality between the $\alpha$- and $\beta$-axis outputs is caused, which results in offset and double-frequency oscillatory errors in the estimated parameters by the LCO-FLL. This is the main shortcoming of the LCO-FLL and can be verified using numerical results. The LCO-FLL also cannot extract the amplitude of its input signal because, as mentioned before, it tries to fix the amplitude of its $\alpha$- and $\beta$-axis outputs at the constant $A$. Besides, it has a limited filtering capability, like the standard SOGI-FLL.

[6]The comb-FLL is basically a self-adaptive recursive discrete Fourier transform (RDFT). The accumulated round-off error problem of the RDFT and its instability issues have been well discussed in the literature [46].

[7]No detailed information about the discretization of the comb-FLL has been presented in [45], and the authors' attempts to obtaining a stable realization of the comb-FLL with the ability to estimate the phase, frequency, and amplitude at the same time have failed. Our simulations show that the comb-FLL can only estimate its input signal frequency. Further investigations on this issue are required.

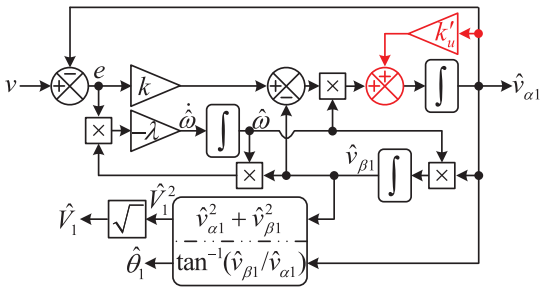


Fig. 16. Block diagram representation of the CLO-FLL [47]. $k'_u = 1 - \hat{V}_1^2$. The nominal value of the input signal amplitude is assumed to be 1 p.u.

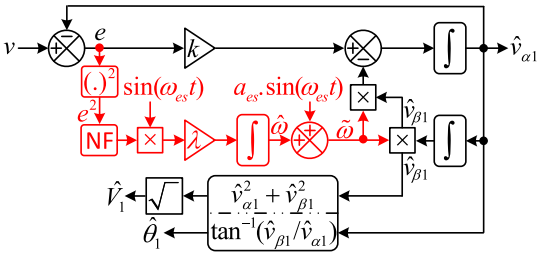


Fig. 17. Block diagram representation of the ES-FLL [49]. $a_{es}$ and $\omega_{es}$ denote the excitation amplitude and angular frequency, respectively. The NF is of second order with a fixed notch frequency at twice the grid nominal frequency.

To deal with some drawbacks of the LCO-FLL, a different structure called the circular limit-cycle oscillator based FLL (CLO-FLL) is proposed in [47]. The block diagram representation of the CLO-FLL is shown in Fig. 16. The CLO-FLL, contrary to the LCO-FLL, can estimate the input signal amplitude. Besides, it does not cause offset/oscillatory errors in the presence of input signal amplitude variations. These characteristics, however, do not demonstrate any superiority over the SOGI-FLL as it already possesses the same features. Indeed, it is demonstrated in [48] that the CLO-FLL and SOGI-FLL offer a close performance as long as the input signal amplitude is at or close to its nominal value.[8]

It is worth mentioning here that the LCO-FLL and CLO-FLL are claimed to be more structurally robust than the SOGI-FLL [10], [47]. Nevertheless, no concrete evidence to support this claim has been provided in [10] and [47]. Working on this issue can be a topic for research.

### H. Extremum-Seeking-Based FLL (ES-FLL)

In [49], a different FLL, called the ES-FLL, is presented. As shown in Fig. 17, the main difference of this FLL compared to the SOGI-FLL lies in its frequency estimator. The basic idea behind developing this estimator is that the square of the error signal $e$ has a local extremum at the grid frequency. Therefore, the extremum seeking control [50], which is an adaptive control method, is applied to minimize the error and extract the grid frequency [49]. This method, as can be seen in Fig. 17, involves feeding a sinusoidal perturbation to the control plant and demodulating the square error with the same frequency component to gain a measure of the gradient information of the system. Notice that a wide-bandwidth non-adaptive NF with the notch frequency at twice the grid nominal frequency is also used before the demodulator to suppress the double-frequency component existing in the signal $e^2$ during transients.

In [49], a dynamic performance comparison between the ES-FLL and SOGI-FLL is performed. The reported results demonstrate that the ES-FLL has no advantage over the SOGI-FLL. Indeed, because of its damped high-frequency oscillations during transients (see [49, Fig. 8]) and the lack of an amplitude normalization in its structure, we may even say that its application causes a relatively poor performance compared to the SOGI-FLL. From the implementation point of view, the ES-FLL is also not an attractive option compared to the SOGI-FLL because, regardless of the additional computational burden caused by the NF and sinusoidal excitation in its structure, it has a more complicated tuning procedure. Notice that the ES-FLL has several more design parameters, which make its tuning a complicated task, at least for those who are not expert in the field.

### I. Summary and Recommendations

Table II summarizes the strengths and weaknesses of the advanced single-phase FLLs discussed before, and Table III summarizes their computational cost. Based on this information, the following recommendations are made.

1) Using the LCO-FLL is not recommended mainly because it is not amplitude adaptive and suffers from oscillatory/offset errors during voltage sags/swells.
2) The CLO-FLL does not demonstrate a considerable performance difference compared to the SOGI-FLL as long as the grid voltage amplitude is at its nominal value. Besides, the lack of an amplitude normalization in its structure makes its dynamics amplitude dependent. For these reasons, its application is not advised.
3) The ES-FLL is not an attractive option mainly because it has a higher computational burden and implementation complexity than the SOGI-FLL and suffers from some damped high-frequency oscillations during transients.
4) Using the comb-FLL is not recommended because, regardless of its high memory requirement at high sampling frequencies, it suffers from a high implementation complexity.
5) The MSOGI-FLL is a good option if the grid harmonic pattern is known and rejecting/extracting few dominant harmonic components is only necessary. It, however, may not be a practical solution for adverse grid scenarios with an unknown harmonic pattern as it involves rejecting a large number of harmonics that causes a huge computational burden. It is worth mentioning here that the dc-offset rejection/estimation loop of the SOGI-FLL-WDCRC (see Fig. 9) may also be included in the MSOGI-FLL structure to make it immune to the dc offset.

[8] As the CLO-FLL has no amplitude normalization, its dynamics are affected by its input signal amplitude variations [48].

TABLE II
STRENGTHS AND WEAKNESSES OF SOME ADVANCED SINGLE-PHASE FLLS

| FLL name | Strengths | Weaknesses | Linear model[1] |
|---|---|---|---|
| **SOGI-FLL-WDCRC** | Perfect extraction/rejection of dc offset<br>Implementation simplicity | Poor harmonic filtering capability[2] | Not available |
| **MSOGI-FLL** | Selective extraction/rejection of harmonics | Poor dc rejection capability[2]<br>Significant computational burden in some grid scenarios[3] | |
| **SOGI-FLL-WPF** | Complete dc offset rejection<br>Rather high attenuation of harmonics | Reduced stability margin compared to the SOGI-FLL | Available |
| **SOGI-FLL-WIF** | Relative implementation simplicity | | |
| **SOGI-FLL-WSS** | Soft startup and smooth phase jump tracking<br>Implementation simplicity | Poor filtering capability[2]<br>High nonlinearity | Not available |
| **Comb-FLL** | High filtering capability | High implementation complexity<br>High memory requirement at high sampling frequencies | |
| **LCO-FLL** | Implementation simplicity | Inability to estimate the amplitude<br>Oscillatory/offset errors under amplitude variations<br>Poor filtering capability[2] | |
| **CLO-FLL** | Implementation simplicity | Amplitude-dependent dynamic behavior<br>Poor filtering capability[2] | Available |
| **ES-FLL** | – – – – – – – – – – | Tuning difficulty<br>Damped high-frequency oscillations during transients<br>Amplitude-dependent dynamic behavior<br>Poor filtering capability[2] | Not available |
| **LKF-FLL** | – – – – – – – – – – | High computational burden<br>Poor harmonic filtering capability[2] | |
| **TD-AFLL** | Very fast dynamic response | Very poor filtering capability<br>Rather high memory requirement at high sampling frequencies | |
| $1\phi$**-CBF-FLL**[4] | Improved filtering capability | Steady-state double-frequency oscillatory errors<br>Frequency offset error at low sampling frequencies<br>Slow dynamic response | Available |

[1] Lack of a linear model implies that an accurate stability analysis and a systematic tuning procedure may not be possible, at least not easily.
[2] A poor dc, harmonic, or generally, filtering capability denotes a filtering ability more or less close to that of the standard SOGI-FLL.
[3] When rejecting/estimating a large number of harmonics is required, the MSOGI-FLL computational burden will be huge, which may not be very practical.
[4] The magnitude of the double-frequency oscillatory errors in the $1\phi$-CBF-FLL, its implementation simplicity/complexity, its transient behavior, and its dc/harmonic filtering capability are affected by the CBF order and bandwidth. For more details, refer to [48] and [51].

TABLE III
COMPUTATIONAL COST OF STANDARD AND ADVANCED SINGLE-PHASE FLLS

| FLL Name | $\times$ | $\div$ | $\pm$ | States | Stored samples[1] | SQRT[2] | ITF[3] | TF[4] |
|---|---|---|---|---|---|---|---|---|
| **Standard SOGI-FLL** | 7 | 2 | 3 | 3 | 0 | 1 | 1 | 0 |
| **SOGI-FLL-WDCRC** | 8 | 2 | 4 | 4 | 0 | 1 | 1 | 0 |
| **MSOGI-FLL**[5] | $7+4n$ | 2 | $3+2n$ | $3+2n$ | 0 | 1 | 1 | 0 |
| **SOGI-FLL-WPF** | 10 | 2 | 5 | 5 | 0 | 1 | 1 | 0 |
| **SOGI-FLL-WIF** | 10 | 2 | 5 | 5 | 0 | 1 | 1 | 0 |
| **SOGI-FLL-WSS** | 9 | 2 | 4 | 3 | 0 | 1 | 1 | 0 |
| **Comb-FLL**[6] | 7 | 3 | 3 | 3 | $T/T_s$ | 1 | 1 | 0 |
| **LCO-FLL** | 9 | 2 | 6 | 3 | 0 | 0 | 1 | 0 |
| **CLO-FLL** | 9 | 1 | 5 | 3 | 0 | 1 | 1 | 0 |
| **ES-FLL** | 11 | 1 | 6 | 5 | 0 | 1 | 1 | 1 |
| **LKF-FLL**[7] | 21 | 2 | 14 | 7 | 0 | 1 | 1 | 0 |
| **TD-AFLL**[7] | 10 | 3 | 5 | 1 | $(T/2)/T_s$ | 1 | 2 | 1 |
| $1\phi$**-CBF-FLL**[8] | 10 | 2 | 6 | 3 | 0 | 1 | 1 | 0 |

[1] **Stored samples** column does not include the required samples for the digital implementation of states (integrators). $T$ denotes a cycle of the fundamental frequency.
[2] **SQRT** means the square root.
[3] **ITF** denotes an inverse trigonometric function.
[4] **TF** denotes a trigonometric function.
[5] $n$ is the number of parallel SOGIs centered at harmonic frequencies.
[6] The computational cost of the comb-FLL does not include the required operations for realizing a variable-length fractional delay.
[7] The LKF-FLL and TD-AFLL are inherently discrete-time algorithms. However, for the sake of consistency, the computational costs of their continuous-time presentations are presented here.
[8] The simplest possible form of the $1\phi$-CBF-FLL, which is based on a first-order CBF, is considered here.

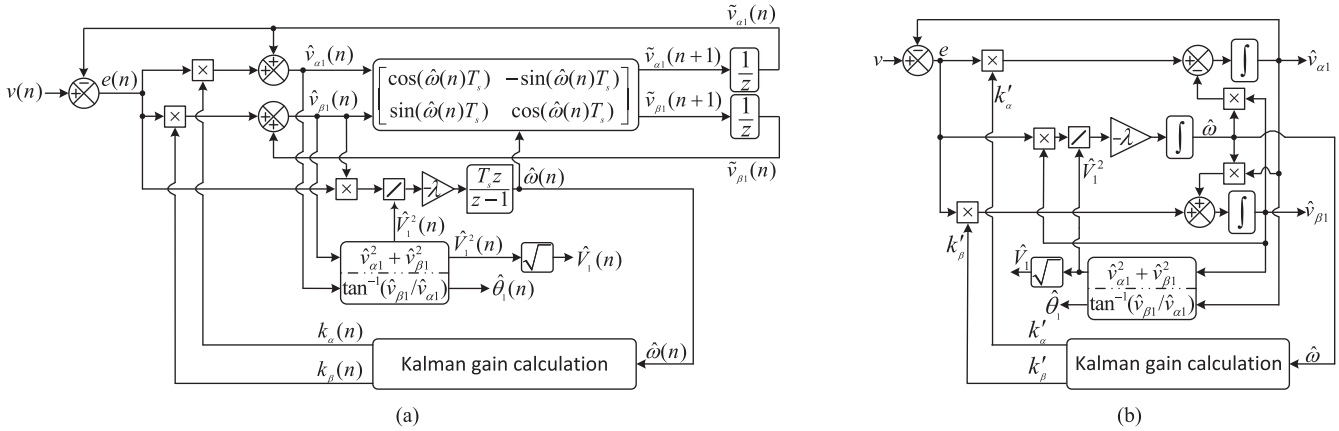


Fig. 18. (a) Block diagram of the LKF-FLL [52]–[54]. (b) Continuous-time representation of the LKF-FLL [48].

6) The SOGI-FLL-WPF and SOGI-FLL-WIF are good options for most grid scenarios as they provide a high filtering capability while maintaining an adequate stability margin, relative implementation simplicity, and acceptable dynamic performance.
7) The adaptive mechanism used in the SOGI-FLL-WSS can be included in all above-mentioned FLLs to enhance their start-up and phase jump tracking operations.

Table II also highlights the availability/unavailability of a linear model for the FLLs under study. Notice that the lack of such a model implies that a careful stability analysis and a systematic parameter tuning may not be possible. Therefore, deriving small-signal models for such FLLs can be a right direction for future works.

## V. Non-SOGI-Based FLLs

Almost all FLLs reviewed so far were based on a SOGI. In this section, some non-SOGI-based approaches for developing a single-phase FLL are reviewed.

### A. Linear-Kalman-Filter-Based FLL (LKF-FLL)

Fig. 18(a) illustrates the block diagram of the LKF-FLL [52]–[54], which inherently is a discrete control algorithm. It includes an LKF for extracting the input signal fundamental component and its quadrature version and a frequency estimator for estimating the input signal frequency. The frequency estimator is the same as that of the SOGI-FLL, and the LKF plays the same role as the SOGI-QSG in the SOGI-FLL. This fact is more evident from Fig. 18(b), which illustrates the continuous-time representation of the LKF-FLL [48].

Regardless of an additional control gain in the $\beta$-axis, the main difference of the LKF-FLL compared to the standard SOGI-FLL is using some computationally demanding recursive equations for updating the Kalman gains. It can be seen in Fig. 18 that the only variable input for the Kalman gain calculation is $\hat{\omega}$. As the grid frequency and, therefore, its estimate (i.e., $\hat{\omega}$) in the steady state experience limited changes around the nominal frequency, it can be concluded that the steady-state values of the Kalman gains have small changes around their corresponding values at the nominal frequency. It implies that the computationally demanding procedure for updating the LKF-FLL Kalman gains has a small effect on its performance. This fact is demonstrated in [48] by performing a numerical comparison between the LKF-FLL and its steady-state version, in which the Kalman gains are fixed. It is also shown in [48] that the LKF-FLL provides a marginal improvement in the dc-offset filtering capability compared to the standard SOGI-FLL. This improvement, nevertheless, may not outweigh the considerable computational effort required for updating the LKF-FLL control gains. It is worth mentioning here that if the procedure for updating the LKF-FLL Kalman gains is ignored and the $\beta$-axis control gain is set to zero, the resultant structure will be mathematically equivalent to the standard SOGI-FLL [48]. The key features of the LKF-FLL and the information about its computational cost are summarized in Tables II and III, respectively.

### B. Transfer-Delay-Based Adaptive FLL (TD-AFLL)

Developing the TD-AFLL [55] is based on the discrete-oscillator law and gradient descent method, as explained in what follows. Assume that the single-phase grid voltage signal in the discrete-time domain is as expressed in (35), in which $m$ and $T_s$ are the current sample and sampling period, respectively, and $V_1$, $\theta_1$, $\varphi_1$, and $\omega$ denote the amplitude, phase angle, initial phase angle, and angular frequency, respectively

$$v(m) = V_1 \cos\overbrace{(m\omega T_s + \varphi_1)}^{\theta_1(m)}. \tag{35}$$

Based on (35), the relationship expressed in (36) can be established between the three equidistant samples of this signal, in which $n$ denotes the distance between samples [56], [57]

$$v(m) + v(m-2n) - 2\underbrace{\cos(nT_s\omega)}_{\sigma} v(m-n) = 0. \tag{36}$$

Using (36), the following cost function may be defined:

$$J = \frac{1}{2}e^2 = \frac{1}{2}[v(m) + v(m-2n) - 2\hat{\sigma}v(m-n)]^2. \tag{37}$$

The gradient descent method can then be applied to (37) to find the update law for estimating $\sigma$ and, therefore, the grid

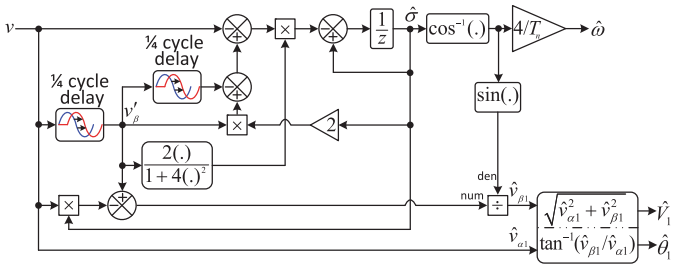


Fig. 19. Block diagram of the TD-AFLL [55].

frequency $\omega$. The result of this procedure with some changes is observed in Fig. 19 [55]. It is referred to as the TD-AFLL [55]. Notice that for estimating the fundamental phase angle and amplitude of the grid voltage, its 90° phase-shifted version is required, which is generated as follows [58]

$$\hat{v}_{\beta 1}(t) = \frac{\overbrace{v(t - T_n/4)}^{v'_\beta(t)} - \cos(T_n\hat{\omega}/4)v(t)}{\sin(T_n\hat{\omega}/4)}. \tag{38}$$

The TD-AFLL benefits from a very fast dynamic response compared to the SOGI-FLL. This advantage, however, comes at the cost of a rather high memory requirement[9] at high sampling frequencies and a very poor filtering capability. Notice that the grid voltage signal and its quadrature version are directly (without any filtering) used for estimating the grid voltage phase and amplitude. Alleviating this problem requires including a prefiltering stage in the input of the TD-AFLL, which increases the implementation complexity and computational burden. Such a prefiltering stage, depending on its dynamics, may also slow down the TD-AFLL transient behavior.

Tables II and III summarize the key features of the TD-AFLL and the information about its computational cost.

### C. Single-Phase Complex Band-pass Filter-Based FLL ($1\phi$-CBF-FLL)

In [51], a dynamical system for estimating the fundamental parameters of a single-phase input signal is presented. Equations (39)–(42) describe this dynamical system in its simplest possible form, and Fig. 20(a) illustrates its block diagram representation

$$\begin{bmatrix}\dot{x}_1\\ \dot{x}_2\end{bmatrix} = \begin{bmatrix}1\\0\end{bmatrix} v - \begin{bmatrix}a & \bar{\omega}\\ -\bar{\omega} & a\end{bmatrix}\begin{bmatrix}x_1\\ x_2\end{bmatrix}$$

$$\begin{bmatrix}\hat{v}_{\alpha 1}\\ \hat{v}_{\beta 1}\end{bmatrix} = c\begin{bmatrix}x_1\\ x_2\end{bmatrix} \tag{39}$$

$$\tilde{\omega} = \frac{\dot{x}_2 x_1 - \dot{x}_1 x_2}{x_1^2 + x_2^2} \tag{40}$$

$$\dot{\hat{\omega}} = \omega_f(\tilde{\omega} - \hat{\omega}) \tag{41}$$

$$\bar{\omega} = \mathrm{sat}(\hat{\omega}). \tag{42}$$

This dynamical system is actually a first-order CBF with a frequency estimator for adjusting its center frequency. Fig. 20(b), which is an alternative mathematically equivalent representation of Fig. 20(a), more clearly illustrates this fact. For this reason, it is referred to as the $1\phi$-CBF-FLL here ($1\phi$ denotes the application for single-phase systems). Notice that the first-order CBF in Fig. 20(b) sees the single-phase input signal as an imbalanced system in the $\alpha\beta$ frame as follows:

$$\begin{aligned} v_\alpha(t) &= \overbrace{V_1\cos(\theta_1)}^{\text{FFPSC}} + \overbrace{V_1\cos(-\theta_1)}^{\text{FFNSC}} = 2v\\ v_\beta(t) &= V_1\sin(\theta_1) + V_1\sin(-\theta_1) = 0 \end{aligned} \tag{43}$$

where FFPSC and FFNSC are abbreviations for the fundamental-frequency positive-sequence component and fundamental-frequency negative-sequence component, respectively. This CBF attenuates the FFNSC and extracts the FFPSC. The FFPSC is then used for estimating the grid frequency and adapting the CBF center frequency to frequency changes.

The first-order CBF in Fig. 20(b) has a limited ability to attenuating the FFNSC. This problem results in double-frequency oscillatory errors in estimating the grid voltage parameters using the $1\phi$-CBF-FLL. To alleviate this problem, one may select a very narrow bandwidth for the CBF. It, however, may not be very practical, as it considerably slows down the dynamic behavior. An alternative approach is using high-order CBFs instead of the first-order one [51]. High-order CBFs, however, demand a higher computational burden.

Another shortcoming of the $1\phi$-CBF-FLL is that using (40) for estimating the input signal frequency results in an offset error [48]. This error depends on the sampling frequency and may become noticeable when the sampling frequency is low.

It is worth mentioning here that a more detailed analysis of the $1\phi$-CBF-FLL and its modeling procedure may be found [48]. The key features of the $1\phi$-CBF-FLL and the information about its computational cost are also summarized in Tables II and III, respectively.

## VI. Some Industrial Applications of Single-Phase FLLs

Besides the grid synchronization, single-phase FLLs have received growing attention in some other industrial applications in recent years. Examples of such applications are presented in this section.

### A. Extraction of Interharmonics

Interharmonics are those disturbances that their frequencies are not integer multiple of the fundamental frequency. They are often caused by the nonlinear interaction between two sources operating at different frequencies. Interharmonics are believed to be more troublesome than harmonics as, in addition to the power quality issues caused by harmonics, they produce some other problems such as subsynchronous oscillations, voltage fluctuations, and light flicker among others [59]. To deal with these problems, the accurate extraction of interharmonics may be required. In what follows, the application of the SOGI-FLL for this purpose is presented.

To this end, a similar approach as that explained in Section IV-B, i.e., using parallel SOGIs, may be used.

[9]Implementing the TD-AFLL requires storing a half-cycle sampled data.

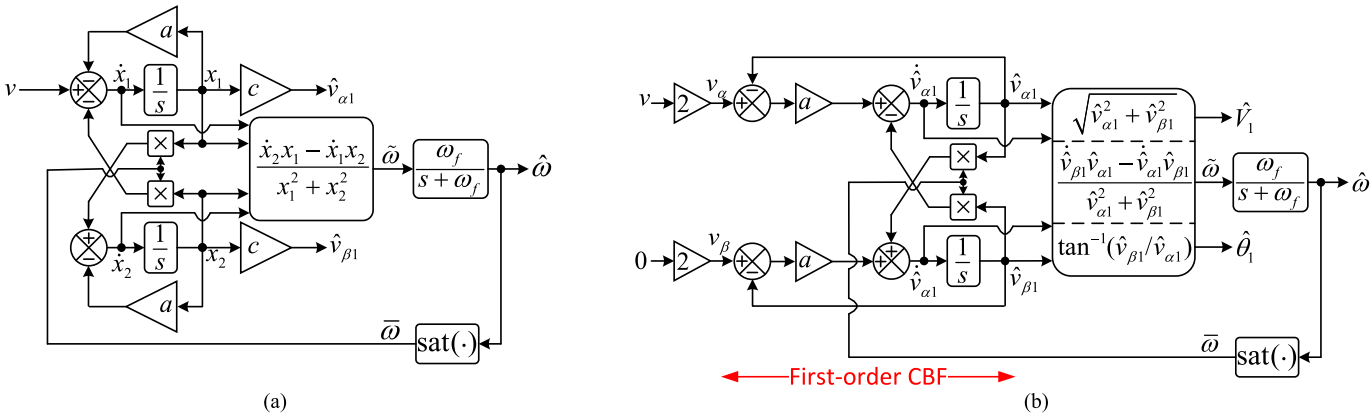


Fig. 20. (a) Simplest possible form of the dynamical system proposed in [51] for estimating the fundamental parameters of a single-phase signal. (b) Its alternative mathematically equivalent representation. For the sake of consistency, the phase and amplitude estimators are also included in this presentation. $\tilde{\omega}$, $\hat{\omega}$, and $\bar{\omega}$ all denote an estimation of the input signal angular frequency. $a$ and $\omega_f$ are design constants and $c = 2a$.

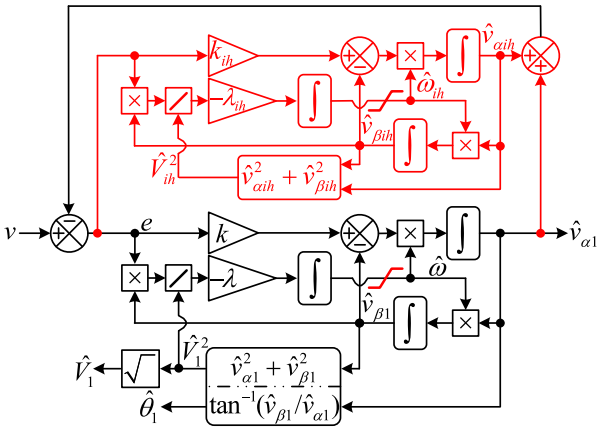

Fig. 21. SOGI-FLL with one interharmonic estimation ability. The subscript $ih$ denotes an interharmonic. This idea has been originally proposed for ANFs [60].

The difference here is that interharmonics have unknown frequencies. Therefore, the parallel SOGIs need to have separate frequency estimators. Fig. 21 illustrates this idea for the simplest possible case, i.e., when estimating only one interharmonic component is required [60]. Notice that, to avoid competition between different units in estimating one component, saturation blocks need to be added to the frequency estimators. The upper and lower limits of each saturation depend on the expected range of variations for the frequency of its corresponding component.

### B. Estimation of Damped Oscillations

In an interconnected power system, low-frequency damped (exponentially decaying) oscillations convey very important information about the system stability, and therefore, extracting their parameters is of high interest. Generating these low-frequency oscillations is attributable to the nonlinear interaction existing among different parts of such a system and also to occurring disturbances. In [16], modifying the SOGI-FLL for extracting the parameters of low-frequency damped (exponentially decaying) oscillations is suggested. This method is explained in what follows.

Equation (44) describes a damped oscillation, in which $v_0$ is the dc component, and $\sigma_d$, $A_d$, $\omega_d$, $\theta_d$, and $\varphi_d$ denote the damping, instantaneous amplitude, angular frequency, phase angle, and initial phase angle, respectively

$$v = v_0 + \overbrace{V_d e^{-\sigma_d t}}^{A_d} \cos\overbrace{(\omega_d t + \varphi_d)}^{\theta_d}. \tag{44}$$

For extracting the parameters of this damped oscillation, the SOGI-FLL-WDCRC [see Fig. 9(a)] is considered as the basic structure. Inspired by the internal model principle, replacing the SOGI by a damped SOGI, $G_{\text{damped-SOGI}}(s) = G_{\text{SOGI}}(s + \sigma_d)$, is then suggested. By applying the gradient descent method,[10] the update law for the damping can be finally obtained as follows:

$$\dot{\hat{\sigma}}_d = -\frac{\gamma}{\hat{A}_d^2} e \hat{v}_{\alpha d}. \tag{45}$$

Fig. 22 illustrates the final product, which is called the damped SOGI-FLL [16]. Notice that if estimating multiple damped oscillations is required, a parallel connection of multiple damped SOGIs with their own frequency/damping estimation loops may be used. Notice also that the dynamic performance of the damped SOGI-FLL may be enhanced by including the adaptive mechanism described in Section IV-E in its frequency and damping estimation loops [16].

A problem of the damped SOGI-FLL is that the estimation may be lost when the dc component is very small or equal to zero, and the input signal is noisy [16]. The reason is that the damped oscillation(s) decays with time, and therefore, the input noise becomes dominant. The damped SOGI-FLL also demonstrates some frequency estimation errors at high frequencies, high damping ratios, and low reporting rates [61]. It is worth

[10] By applying the gradient descent method, a factor of $t$ also appears in the update law for the damping, which is neglected to avoid instability [27]. To ensure an amplitude independence, the amplitude normalization is also included in the update law.

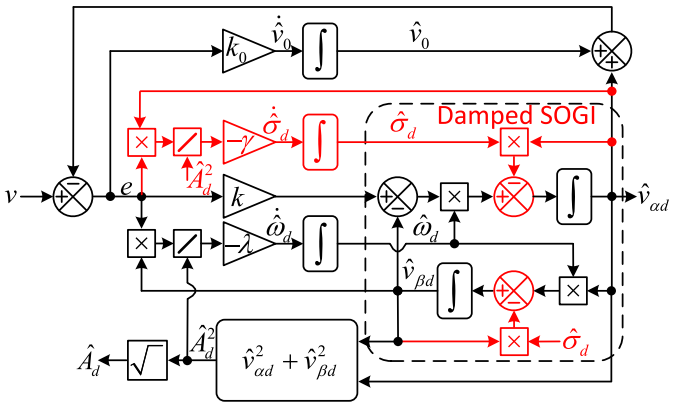


Fig. 22. Damped SOGI-FLL [16].

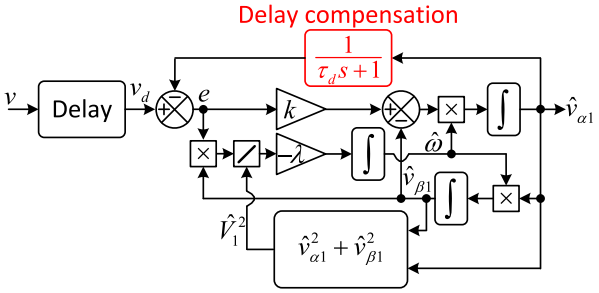


Fig. 23. SOGI-FLL with the delay compensation capability. This idea has been originally proposed for three-phase applications in [63].

mentioning here that no accurate small-signal model for the damped SOGI-FLL has yet been presented.

### C. Delay Compensation

The measurement and control delays may adversely affect the performance and stability of power converters, particularly in high-power converters that have a low switching frequency [62]. To deal with this problem, different approaches have been proposed. In [63], a simple yet effective method based on the SOGI-FLL is proposed. This approach is briefly explained in what follows.

Assume that the signal $v$ is the signal to which we need to be synchronized. Also, assume that we do not have access to this signal, and only its delayed version is available. For a small delay, the relation between these signals can be expressed as

$$v_d(s) = e^{-\tau_d s} v(s) \approx \frac{1}{\tau_d s + 1} v(s) \tag{46}$$

where $\tau_d$ denotes the aforementioned delay and is assumed to be known, and $v_d$ is the delayed version of $v$. To compensate for this delay and generate a synchronized signal with $v$, its delayed version is considered as the SOGI-FLL input and a first-order LPF with a time constant equal to $\tau_d$ is included in the SOGI-FLL feedback loop [63]. In this way, the same delay as that existing between $v$ and $v_d$ is created in the feedback signal and, therefore, compensates for the SOGI-FLL input delay. Fig. 23 illustrates this idea [63].

### D. Delay Estimation Between Two or More Versions of a Signal

In a large number of industrial applications, estimating the delay(s) between two or more versions of the same signal received at spatially separated sensors is required. The earthquake center determination, speed sensing, speech enhancement, and communication receiver synchronization are examples of such applications. Over the past 20 years, different algorithms have been developed to deal with this problem. Recently, modifying the SOGI-FLL structure to address this problem has been proposed in [17]. This method is briefly explained in what follows.

Assume that $v$ and $v_d$ are two versions of the same signal, and there is an unknown time delay equal to $\tau_d$ between them, i.e., $v_d(t) = v(t - \tau_d)$. Also, assume that the signal $v$ is as (3). Therefore, the signal $v_d$ may be expressed as

$$v_d(t) = V_1 \cos(\theta_1 - \omega \tau_d). \tag{47}$$

Notice that the input signal amplitude is assumed to be constant.

As shown in Fig. 24, the filtered in-phase and quadrature-phase versions of the signal $v$ (i.e., $\hat{v}_{\alpha 1}$ and $\hat{v}_{\beta 1}$) and its angular frequency are extracted using a standard SOGI-FLL. Using this information and assuming that $\hat{\tau}_d$ is an estimation of $\tau_d$, an estimation of the signal $v_d$ and its 90° phase-shifted version may be provided, as expressed in the following:

$$\begin{bmatrix} \hat{v}_d \\ \hat{v}_q \end{bmatrix} = \begin{bmatrix} \cos(\hat{\omega}\hat{\tau}_d) & \sin(\hat{\omega}\hat{\tau}_d) \\ -\sin(\hat{\omega}\hat{\tau}_d) & \cos(\hat{\omega}\hat{\tau}_d) \end{bmatrix} \begin{bmatrix} \hat{v}_{\alpha 1} \\ \hat{v}_{\beta 1} \end{bmatrix} = \begin{bmatrix} \hat{V}_1 \cos(\hat{\theta}_1 - \hat{\omega}\hat{\tau}_d) \\ \hat{V}_1 \sin(\hat{\theta}_1 - \hat{\omega}\hat{\tau}_d) \end{bmatrix}. \tag{48}$$

Using (47) and (48), the cost function (49) can be defined as

$$J = \frac{1}{2} e_d^2 = \frac{1}{2} [v_d - \hat{v}_d]^2 = \frac{1}{2} [V_1 \cos(\theta_1 - \omega \tau_d) - \hat{V}_1 \cos(\hat{\theta}_1 - \hat{\omega}\hat{\tau}_d)]^2. \tag{49}$$

By applying the gradient descent method to (49), the update law for $\tau_d$ is obtained as[11]

$$\dot{\hat{\tau}}_d = -\mu' \frac{\delta J}{\delta \hat{\tau}_d} = \mu \hat{v}_q [v_d - \hat{v}_d]. \tag{50}$$

Fig. 23 illustrates the delay estimation between two signals using the SOGI-FLL [17]. This structure can be simply extended to any number of signals.

### E. Implementation of an Efficient Differentiator/Integrator

Differentiators/integrators are basic building blocks of control systems in different industrial applications. Depending on the application at hand, these elements can be implemented in different ways. In most industrial applications, using ordinary differentiators/integrators is good enough. There are, however, applications in which more efficient differentiators/integrators

[11] A factor of frequency also appears in the time-delay update law, which is absorbed into the step-size parameter.

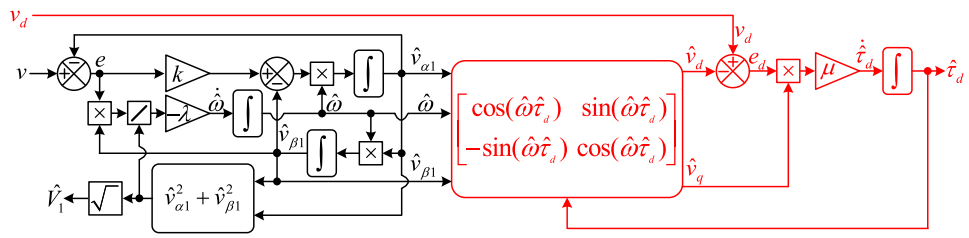


Fig. 24. Delay estimation between two sinusoidal signals using the SOGI-FLL [17].

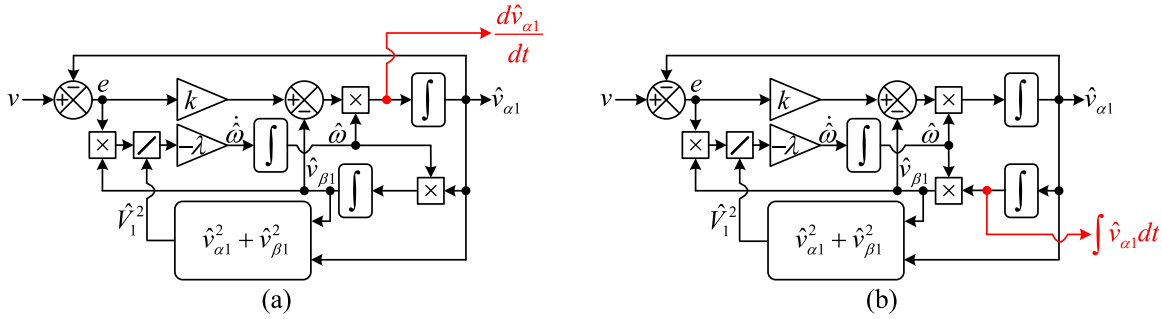


Fig. 25. (a) SOGI-FLL-based differentiator. (b) SOGI-FLL-based integrator.

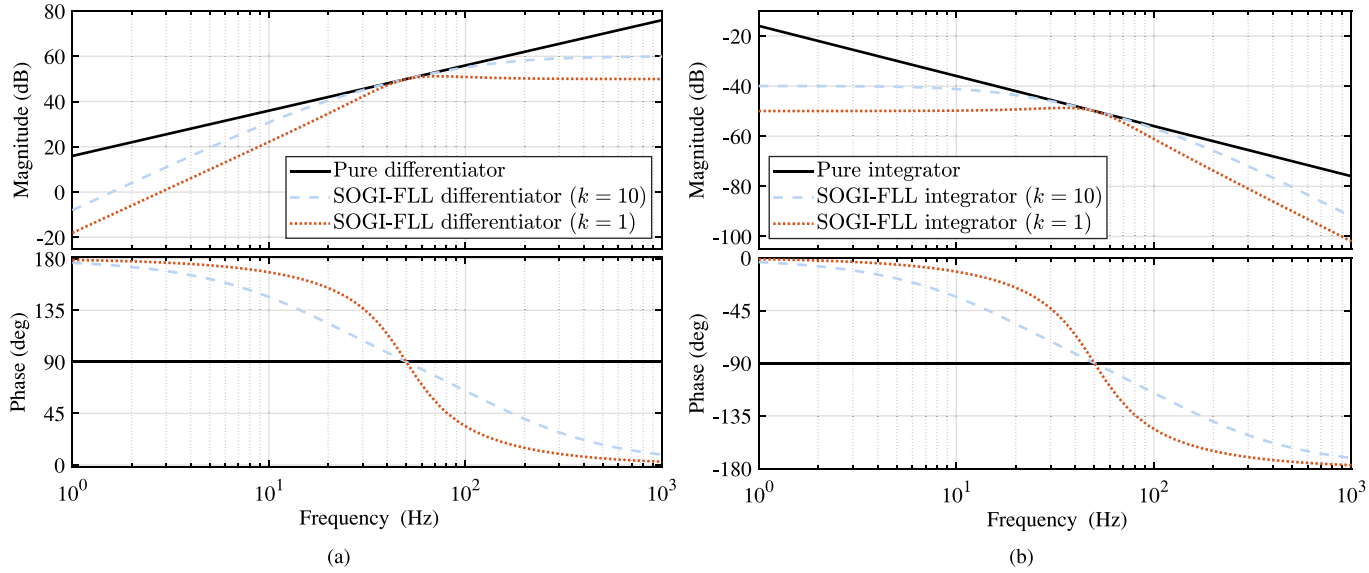


Fig. 26. (a) Frequency response of the pure and SOGI-FLL-based differentiators. (b) Frequency response of the pure and SOGI-FLL-based integrators.

are demanded. For instance, in a noisy environment, employing an ordinary differentiator (which is usually implemented using the backward Euler method) may not be very practical as it causes noise amplification. And using an ordinary integrator may not be practical for integrating sinusoidal signals with a dc component as it results in the integrator saturation. The capacitor voltage active damping in *LCL*-filtered grid-tied power converters [64], in which the time differentiation of the capacitor voltage is required for the active damping, and the flux estimation in electrical motors [14], which involves integrating the back electromotive force, are well-known examples of such scenarios.

To address the aforementioned problems, using the SOGI-FLL for designing more efficient differentiators and integrators has been proposed recently [14], [64], [65]. The key point in designing such a differentiator/integrator is that the $\alpha$-axis output of the SOGI-FLL is a filtered version of the fundamental component of its input. Therefore, the highlighted points in Fig. 25 give the derivative and integral of the input signal at the fundamental frequency.

Fig. 26 illustrates the frequency responses of the SOGI-FLL-based and pure differentiators and integrators. Based on these Bode plots, the following observations are made.

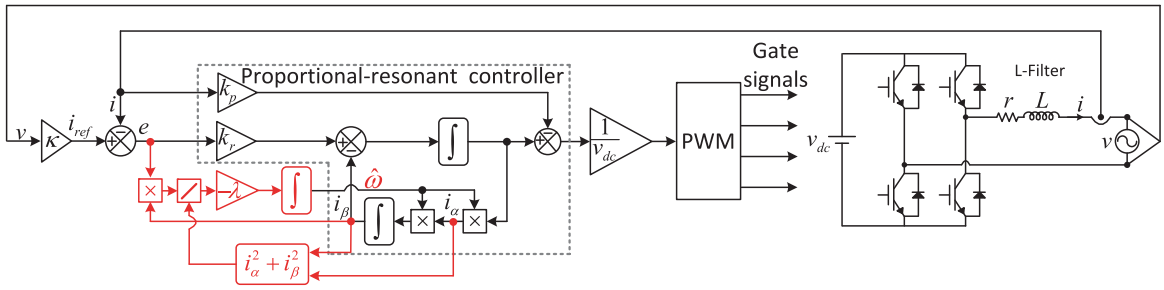


Fig. 27. Single-phase grid-connected inverter with an adaptive resonant controller [11].

1) The SOGI-FLL-based differentiator (integrator) has the same magnitude and phase as the pure differentiator (integrator) at the fundamental frequency, which means it is a frequency-selective differentiator (integrator).
2) The magnitude-frequency response of the SOGI-FLL-based differentiator (integrator) becomes flat at frequencies higher (lower) than the fundamental frequency and, consequently, faces a less high-frequency noise (dc) problem compared to a pure differentiator (integrator).
3) The frequency response of the SOGI-FLL-based differentiator (integrator) may become more close to that of a pure differentiator (integrator) around the fundamental frequency by increasing the control gain $k$.

Notice that the dc-offset problem in the SOGI-FLL-based integrator can be completely solved by including the dc-offset estimation/rejection loop into the SOGI-FLL structure, as shown in Fig. 9. Notice also that if differentiating/integrating from multiple frequency components of a signal at the same time is required, the concept of parallel SOGIs (see Fig. 10) may be used.

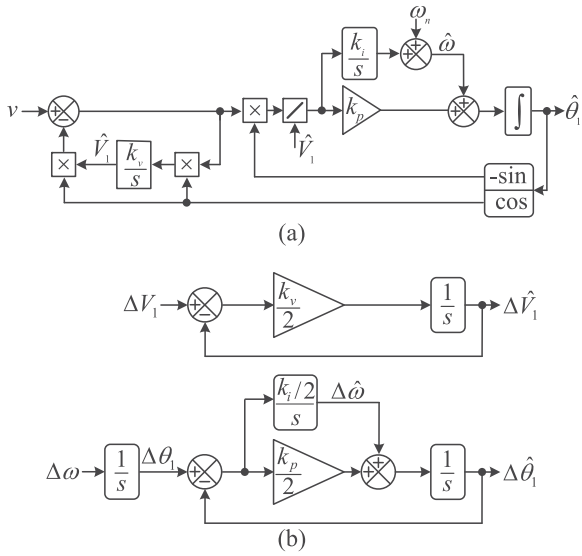


Fig. 28. (a) EPLL. (b) Its LTI model.

### *F. Design of Adaptive Resonant Controllers*

Resonant controllers are highly popular for the control of power converters as they guarantee a zero tracking error for the converter without any requirement for transferring the information to the synchronous reference frame. A hidden assumption here is that the grid frequency is fixed at its nominal value. This assumption, however, may not always be valid, particularly when the converter is connected to a weak grid. In this case, the center frequency of the resonant controller needs to be adapted to the grid frequency changes. When the converter has a dedicated synchronization technique like a PLL, there is no problem as an estimation of the grid frequency is always provided by the synchronization part. Nevertheless, a tracking error may happen when there is no synchronization unit in the control strategy. An example of such controllers, which are characterized by having a simpler and more compact structure compared to the PLL-based ones, can be found in [66] and [67]. In this controller, the converter reference current is directly generated from the grid voltage as $i_{\text{ref}} = \kappa v$ ($\kappa$ is the output signal of the dc-link voltage controller). In this way, the reference current is synchronized with the grid voltage without any synchronization unit. Nevertheless, because of having no information about the grid frequency, the center frequency of the resonant controller is fixed at the nominal frequency, which results in a tracking error under off-nominal frequencies. Addressing this tracking error for single-phase grid-tied power converters is presented in [11].

The key idea is that a resonant controller is actually a GI. Therefore, adapting its center frequency to frequency changes should be possible by using the same frequency estimator as that of the SOGI-FLL and ANFs. Fig. 27 illustrates this idea [11], in which the additional frequency estimator is highlighted. It is demonstrated using experimental results in [11] that this additional frequency detector effectively extracts the grid frequency and, therefore, prevents a tracking error under off-nominal frequencies. An accurate model for describing the frequency estimation dynamics is also presented in [11], which considerably facilitates the tuning procedure. It is worth mentioning here that a harmonic compensator, which includes multiple parallel resonant controllers tuned at the concerned harmonic frequencies, may also be added to the proportional-resonant controller in Fig. 27 to enhance its disturbance rejection capability.

## VII. Connection Between Single-Phase FLLs and PLLs

Despite some efforts to clarify the relation between single-phase PLLs and FLLs [28], [42], [68], articles are still full of

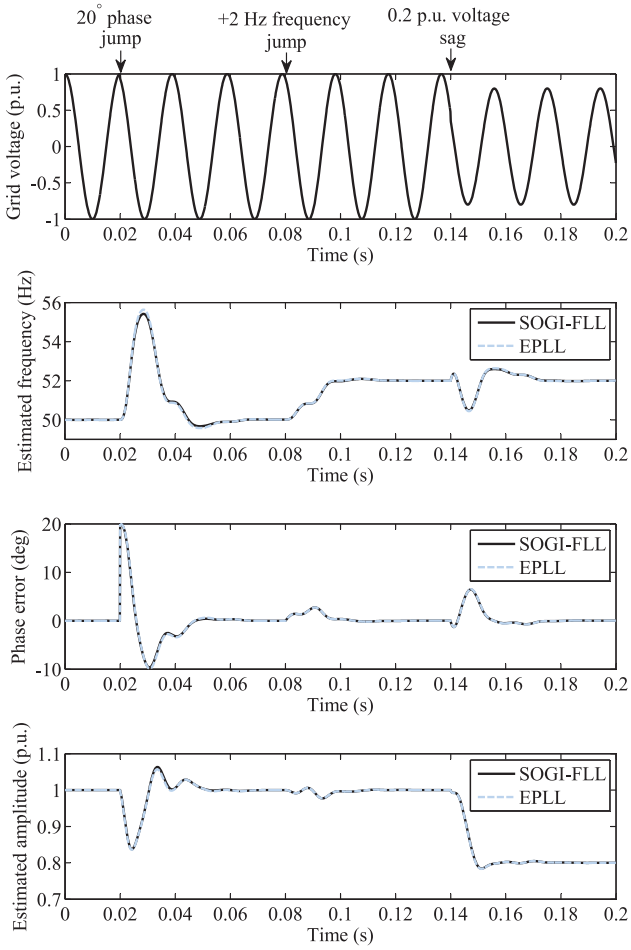


Fig. 29. Performance comparison between the SOGI-FLL and the EPLL in response to different tests. The SOGI-FLL parameters are $k = \sqrt{2}$ and $\lambda = 49348$. The EPLL parameters are $k_p = k_v = k\omega_n = 444.3$ and $k_i = \lambda = 49348$.

contradictory remarks about these synchronization techniques. The aim of this section is to put an end to this argument. To this end, the SOGI-FLL, which is a standard FLL and a basic structure for implementing most advanced single-phase FLLs, and the enhanced PLL (EPLL) [42], [68], which is a well-known and popular single-phase PLL, are considered. Fig. 28(a) illustrates the block diagram of the EPLL. $k_p$, $k_i$, and $k_v$ are the control parameters of the EPLL. It is worth mentioning here that developing this PLL, similar to the SOGI-FLL, can be carried out by applying the gradient descent method.

The performance comparison of the SOGI-FLL and EPLL should be carried out under a fair condition. An easy yet effective way to find such a condition is obtaining the EPLL model and comparing it with that of the SOGI-FLL. Fig. 28(b) illustrates the EPLL LTI model, which can be readily obtained by considering (3) as the EPLL input signal and assuming a quasi-locked state. Comparing the LTI model of the EPLL [see Fig. 28(b)] with that of the SOGI-FLL [see Fig. 4] gives the fair condition of comparison as $k_p = k_v = k\omega_n$ and $k_i = \lambda$.

Fig. 29 compares the performance of the SOGI-FLL and EPLL in response to a 20° phase jump, a 2-Hz frequency jump, and a 0.2-p.u. voltage sag under the aforementioned condition

TABLE IV
COMPUTATIONAL COST OF THE STANDARD SOGI-FLL AND EPLL

| FLL Name | × | ÷ | ± | States | SQRT | ITF | TF |
|---|---|---|---|---|---|---|---|
| **Standard SOGI-FLL** | 7 | 2 | 3 | 3 | 1 | 1 | 0 |
| **EPLL** | 6 | 1 | 3 | 3 | 0 | 0 | 2 |

TABLE V
INTEGRATOR DISCRETIZATION METHODS

| Discretization Method | Equivalence |
|---|---|
| **Forward Euler** | $\frac{1}{s} = \frac{T_s z^{-1}}{1-z^{-1}}$ |
| **Backward Euler** | $\frac{1}{s} = \frac{T_s}{1-z^{-1}}$ |
| **Tustin** | $\frac{1}{s} = \frac{T_s}{2}\frac{1+z^{-1}}{1-z^{-1}}$ |
| **Tustin with pre-warping** | $\frac{1}{s} = \frac{\tan(\hat{\omega}T_s/2)}{\hat{\omega}}\frac{1+z^{-1}}{1-z^{-1}}$ |
| **Third-order integrator** | $\frac{1}{s} = \frac{T_s}{12}\frac{23z^{-1}-16z^{-2}+5z^{-3}}{1-z^{-1}}$ |

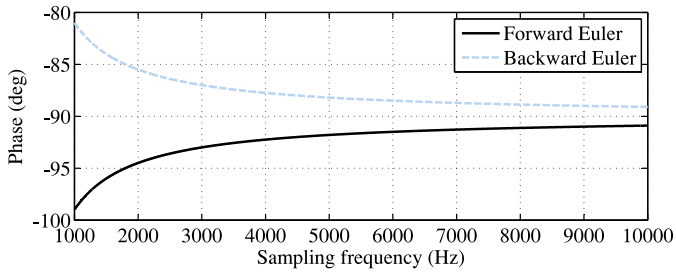


Fig. 30. Phase response of an integrator discretized using forward and backward Euler methods at the fundamental frequency (50 Hz) versus the sampling frequency.

for their control parameters. As expected, they demonstrate almost identical results, which imply they are mathematically equivalent. A mathematical proof of this equivalence may also be found in [68]. Considering this equivalence, it can be concluded that almost all advanced FLLs described in Section IV may also be realized by using the EPLL (for some examples, refer to [5]). It is also worth mentioning here that the EPLL is equivalent to or has a close relationship with some well-known single-phase PLLs, such as the inverse park PLL and the synthesis circuit PLL (also called the simplest $1\varphi$-SRF-PLL) among others [69]. It means that the SOGI-FLL is also equivalent to or has a close relationship with them.

From a practical implementation point of view, however, the SOGI-FLL and EPLL have some differences. The first is that the EPLL demonstrates more robustness compared to the SOGI-FLL when the sampling frequency is very low [61], [68], [70].[12] The reason is that integrators of the EPLL act on dc signals. The two integrators of the SOGI in the SOGI-FLL, however, operate on ac signals and, therefore, require a higher sampling rate. The second difference lies in using different functions in their implementation. In the EPLL, the calculation of sine and cosine functions is required. However, in the SOGI-FLL, the computa-

[12] A hidden assumption here is that no trigonometric function is used in the discretization of the SOGI-FLL.

tion of the square root and inverse tangent function is demanded (see Table IV for more details). Notice that the EPLL directly provides a synchronized signal with a unity amplitude. Generating such signals in the SOGI-FLL, however, demands dividing its $\alpha$- and $\beta$-axis outputs by the estimated amplitude, which causes a bit more computational burden. Of course, in applications where only a synchronized signal with a unity amplitude is required, the inverse tangent calculation in the SOGI-FLL can be avoided, which is an advantage from the computational point of view. And finally, the EPLL offers higher robustness compared to the SOGI-FLL in the fixed-point implementation. This fact can be concluded from discussions conducted in [71].

## VIII. Discretization Aspects

The implementation of the SOGI-FLL in a digital signal processor involves its discretization. This task can be carried out in different ways. Using the backward Euler, forward Euler, a combination of backward and forward Euler, Tustin, Tustin with prewarping, and third-order Adams-Bashforth method (also known as the third-order integrator) are typical choices [72]–[75]. Before analyzing these approaches, the requirements of an efficient discretized version of the SOGI-FLL are first explained in what follows.

1) Assuming that $G_\alpha(z)$ and $G_\beta(z)$ are the resultant $z$-domain transfer functions between the $\alpha$- and $\beta$-axis outputs of the SOGI-QSG and the grid voltage, respectively, their frequency responses at the fundamental frequency should have the following specifications:
$$\begin{aligned} &\left|G_\alpha(e^{j\omega_n T_s})\right| = \left|G_\beta(e^{j\omega_n T_s})\right| = 1 \\ &\angle G_\alpha(e^{j\omega_n T_s}) = 0^\circ \\ &\angle G_\beta(e^{j\omega_n T_s}) = -90^\circ \end{aligned} \tag{51}$$
where $|.|$ and $\angle.$ denote the magnitude and phase, respectively. This requirement implies that there should be $90^\circ$ phase difference between the $\alpha$- and $\beta$-axis outputs at the fundamental frequency.
2) The computational burden should be minimized. This suggests that a discretization method that involves computing trigonometric function(s) may not be a very good option. Notice that avoiding the calculation of trigonometric functions has been the main motivation in developing the SOGI-FLL. Notice also that we already have an efficient trigonometric-function-based implementation of the SOGI-FLL, known as the EPLL (see Section VII), which offers high structural robustness in fixed-point implementations and at low sampling frequencies.
3) The implementation simplicity should be preserved, and no algebraic loop should happen.

According to the above-mentioned requirements and Fig. 30, which illustrates the fundamental-frequency phase response of an integrator discretized using the forward and backward Euler methods as a function of the sampling frequency, it can be concluded that these approaches are not good options for the SOGI discretization. Notice that, as shown in Fig. 30, these discretization methods are not able to provide an exactly $-90^\circ$ phase at the fundamental frequency [72].[13] This is particularly true when the sampling frequency is low. Therefore, their application for the SOGI discretization results in a nonorthogonality between the $\alpha$- and $\beta$-axis outputs and, therefore, some errors in the estimated parameters by the SOGI-FLL.

Employing the Tustin method for the SOGI discretization also involves some difficulties. The first challenge is that its direct application for the SOGI discretization (i.e., approximating two integrators of the SOGI with the Tustin method) results in algebraic loops [72]. To avoid this problem, one may discretize the closed-loop transfer functions of the SOGI-QSG, i.e., (1) and (2) [72]. The second problem is that, as shown using solid black lines in Fig. 31, using the Tustin method fails to effectively fulfill the requirements summarized in (51) at low sampling frequencies. To deal with this challenge, one may use the Tustin with prewarping method [74] (see gray dashed lines in Fig. 31), but at the cost of calculating an additional trigonometric function.

The third-order Adam–Bashforth method, contrary to the Tustin method, is directly applicable for the SOGI discretization. This feature has made it very popular for discretizing advanced FLLs, particularly those that are based on more than one SOGI [6]. This approach, however, similar to the Tustin method, results in some inaccuracies at low sampling frequencies. The dotted lines in Fig. 31 illustrate this fact.

The key points of the above-mentioned information are summarized in what follows.

1) Using forward and backward Euler methods for the SOGI discretization is not recommended mainly because they result in a noticeable nonorthogonality between the $\alpha$- and $\beta$-axis outputs, even when the sampling frequency is high.
2) The third-order Adam–Bashforth and Tustin methods are both efficient for the discretization at high sampling frequencies. The former one, however, is more a convenient approach because it is directly applicable for the SOGI discretization. This is particularly true when the discretization of advanced FLLs with multiple SOGIs is intended.
3) At low sampling frequencies, the Tustin with prewarping method offers a remarkable accuracy. Its application, however, may not be very convenient for the discretization of advanced FLLs. Considering the high robustness of the EPLL at low sampling frequencies, which is an alternative implementation of the standard SOGI-FLL, these advanced FLLs may be realized using the EPLL concept.

## IX. Summary and Conclusion

In this paper, a review of recent advances in designing single-phase FLLs was presented. In Section II, the historical development of the SOGI-FLL from a nonadaptive SOGI-QSG to its final version was explained. The available linear models for the SOGI-FLL, i.e., the first-order LTI model (see Fig. 3), the second-order LTI model (see Fig. 4), and the LTP model (see Fig. 5) were then demonstrated. The second-order LTI model is

[13] It is not the only problem of using the forward and backward Euler methods for the SOGI-FLL discretization. This problem, however, is serious enough to conclude that they are not a good option.

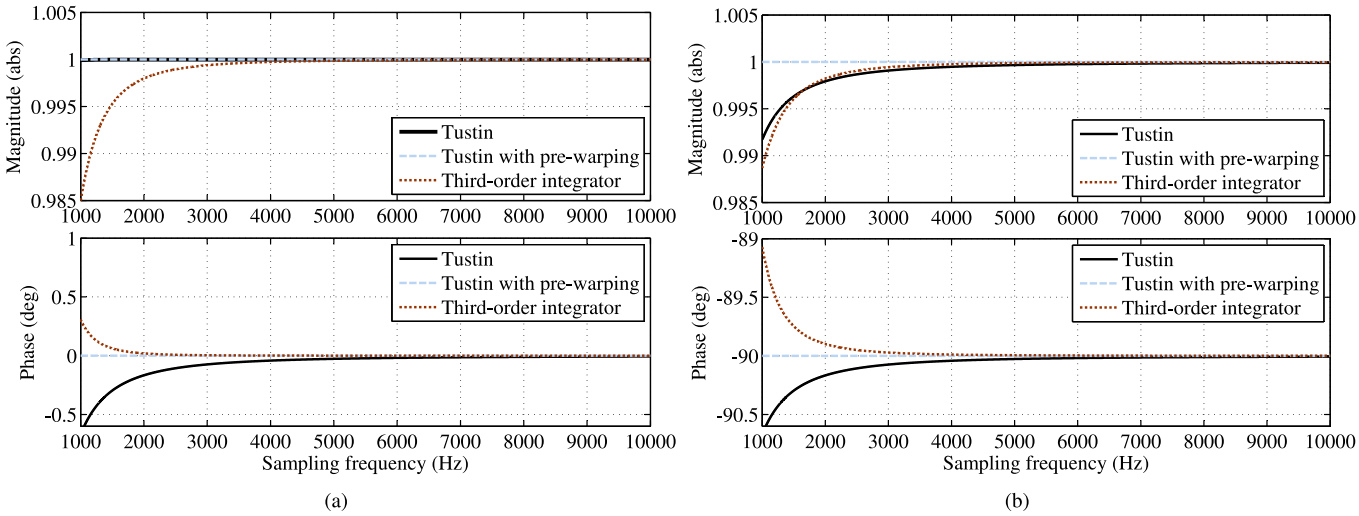


Fig. 31. Fundamental-frequency response of the characteristic transfer functions of the SOGI-QSG discretized using Tustin, Tustin with prewarping, and third-order Adam–Bashforth methods as a function of the sampling frequency. (a) Transfer function (1). (b) Transfer function (2). The parameter $k$ is equal to $\sqrt{2}$.

recommended as the best choice here, as it gives a satisfactory compromise between the accuracy and simplicity of analysis. Using the first-order model is not recommended as it cannot even predict the average dynamic behavior of the SOGI-FLL. The LTP model provides great accuracy, but its analysis is more complicated than the LTI model. Therefore, it can be used for a more thorough analysis of the SOGI-FLL, particularly when there are some stability concerns.

In Section III, the historical development of ANFs was briefly explained, and the close relationship between them and SOGI-FLL was highlighted. Although experts in the field already know this close relationship, it was necessary to be emphasized again in this work as some researchers are not well aware of this fact. Reporting different results for the SOGI-FLL and ANFs in some recent publications confirms this lack of knowledge.

In Sections IV and V, a review of advanced single-phase SOGI-based and non-SOGI-based FLLs for the grid synchronization purposes was conducted, respectively. The common objective in designing these FLLs is improving the standard SOGI-FLL performance, particularly its filtering capability. The operating principles of these FLLs were explained, and their advantages/disadvantages were briefly discussed.

In Section VI, some industrial applications of single-phase FLLs were presented. These applications include extracting interharmonics, estimating electromechanical oscillations, delay compensation in power converters, estimating the delay between two or more versions of a signal, implementing efficient frequency-selective differentiators and integrators, and designing frequency-adaptive resonant controllers for single-phase grid-tied power converters. Advantages/disadvantages of applying single-phase FLLs in these applications were briefly explained.

In Section VII, the connection between single-phase FLLs and PLLs was discussed. The standard SOGI-FLL and EPLL were considered as case studies. It was discussed that they are mathematically equivalent systems if a certain condition holds. It implies that almost all advanced single-phase FLLs described in Section IV may also be realized using the EPLL. It also means that the SOGI-FLL is equivalent or at least has a close relationship with several other single-phase PLLs (e.g., the inverse park PLL and synthesis circuit PLL) because it has already been proved that these PLLs have such a close relationship with the EPLL.

Finally, in Section VIII, the discretization aspects of the SOGI-FLL were covered. It was discussed that the forward and backward Euler methods are not good options for the SOGI discretization as they result in considerable errors, even at high sampling frequencies. The Tustin and third-order Adams–Bashforth methods are right choices as long as the sampling frequency is high. At low sampling frequencies, one may apply the Tustin with prewarping method or use the EPLL concept, but at the cost of computing trigonometric function(s).

This work provides good insight into the standard single-phase SOGI-FLL, its modeling and tuning, its advanced versions for the grid synchronization and other industrial applications, its connection with ANFs and PLLs, and its discretization aspects. Therefore, it can be a useful reference for researchers, particularly those who have limited knowledge and interested in making further contributions to the field. It may also be beneficial for engineers as FLLs have been proven to be a handy tool for different signal processing/control applications.

## REFERENCES

[1] S. Golestan, A. Vidal, A. G. Yepes, J. M. Guerrero, J. C. Vasquez, and J. Doval-Gandoy, "A true open-loop synchronization technique," *IEEE Trans. Ind. Inform.*, vol. 12, no. 3, pp. 1093–1103, Jun. 2016.

[2] F. D. Freijedo, J. Doval-Gandoy, O. Lopez, and E. Acha, "A generic open-loop algorithm for three-phase grid voltage/current synchronization with particular reference to phase, frequency, and amplitude estimation," *IEEE Trans. Power Electron.*, vol. 24, no. 1, pp. 94–107, Jan. 2009.

[3] S. Golestan, J. M. Guerrero, and J. C. Vasquez, "Three-phase PLLs: A review of recent advances," *IEEE Trans. Power Electron.*, vol. 32, no. 3, pp. 1894–1907, Mar. 2017.

[4] S. Golestan, J. M. Guerrero, and J. C. Vasquez, "Single-phase PLLs: A review of recent advances," *IEEE Trans. Power Electron.*, vol. 32, no. 12, pp. 9013–9030, Dec. 2017.

[5] M. Karimi-Ghartemani, *Enhanced Phase-Locked Loop Structures for Power and Energy Applications*. Hoboken, NJ, USA: Wiley, 2014.

[6] P. Rodriguez, A. Luna, I. Candela, R. Mujal, R. Teodorescu, and F. Blaabjerg, "Multiresonant frequency-locked loop for grid synchronization of power converters under distorted grid conditions," *IEEE Trans. Ind. Electron.*, vol. 58, no. 1, pp. 127–138, Jan. 2011.

[7] S. Golestan, J. M. Guerrero, J. C. Vasquez, A. M. Abusorrah, and Y. Al-Turki, "Modeling, tuning, and performance comparison of second-order-generalized-integrator-based FLLs," *IEEE Trans. Power Electron.*, vol. 33, no. 12, pp. 10229–10239, Dec. 2018.

[8] D. Yazdani, A. Bakhshai, G. Joos, and M. Mojiri, "A nonlinear adaptive synchronization technique for grid-connected distributed energy sources," *IEEE Trans. Power Electron.*, vol. 23, no. 4, pp. 2181–2186, Jul. 2008.

[9] P. Rodriguez, A. Luna, R. S. Munoz-Aguilar, I. Etxeberria-Otadui, R. Teodorescu, and F. Blaabjerg, "A stationary reference frame grid synchronization system for three-phase grid-connected power converters under adverse grid conditions," *IEEE Trans. Power Electron.*, vol. 27, no. 1, pp. 99–112, Jan. 2012.

[10] E. Oviedo, N. Vazquez, and R. Femat, "Synchronization technique of grid-connected power converters based on a limit cycle oscillator," *IEEE Trans. Ind. Electron.*, vol. 65, no. 1, pp. 709–717, Jan. 2018.

[11] S. Golestan, E. Ebrahimzadeh, J. M. Guerrero, and J. C. Vasquez, "An adaptive resonant regulator for single-phase grid-tied VSCs," *IEEE Trans. Power Electron.*, vol. 33, no. 3, pp. 1867–1873, Mar. 2018.

[12] Q. Sun, J. M. Guerrero, T. Jing, J. C. Vasquez, and R. Yang, "An islanding detection method by using frequency positive feedback based on FLL for single-phase microgrid," *IEEE Trans. Smart Grid*, vol. 8, no. 4, pp. 1821–1830, Jul. 2017.

[13] W. Xu, Y. Jiang, C. Mu, and F. Blaabjerg, "Improved nonlinear flux observer-based second-order SOIFO for PMSM sensorless control," *IEEE Trans. Power Electron.*, vol. 34, no. 1, pp. 565–579, Jan. 2019.

[14] Z. Xin, R. Zhao, F. Blaabjerg, L. Zhang, and P. C. Loh, "An improved flux observer for field-oriented control of induction motors based on dual second-order generalized integrator frequency-locked loop," *IEEE J. Emerg. Sel. Topics Power Electron.*, vol. 5, no. 1, pp. 513–525, Mar. 2017.

[15] R. Zhao, Z. Xin, P. C. Loh, and F. Blaabjerg, "A novel flux estimator based on multiple second-order generalized integrators and frequency-locked loop for induction motor drives," *IEEE Trans. Power Electron.*, vol. 32, no. 8, pp. 6286–6296, Aug. 2017.

[16] M. Mansouri, M. Mojiri, M. A. Ghadiri-Modarres, and M. Karimi-Ghartemani, "Estimation of electromechanical oscillations from phasor measurements using second-order generalized integrator," *IEEE Trans. Instrum. Meas.*, vol. 64, no. 4, pp. 943–950, Apr. 2015.

[17] M. Ghadiri-Modarres, M. Mojiri, and M. Karimi-Ghartemani, "New adaptive algorithm for delay estimation of sinusoidal signals with unknown frequency," *IEEE Trans. Instrum. Meas.*, vol. 64, no. 9, pp. 2360–2366, Sep. 2015.

[18] M. Mojiri, M. Karimi-Ghartemani, and A. Bakhshai, "Time-domain signal analysis using adaptive notch filter," *IEEE Trans. Signal Process.*, vol. 55, no. 1, pp. 85–93, Jan. 2007.

[19] M. Mojiri and A. Bakhshai, "Estimation of $n$ frequencies using adaptive notch filter," *IEEE Trans. Circuits Syst. II, Express Briefs,*, vol. 54, no. 4, pp. 338–342, Apr. 2007.

[20] D. Yazdani, M. Mojiri, A. Bakhshai, and G. Joos, "A fast and accurate synchronization technique for extraction of symmetrical components," *IEEE Trans. Power Electron.*, vol. 24, no. 3, pp. 674–684, Mar. 2009.

[21] Y. D. Lin and Y. H. Hu, "Power-line interference detection and suppression in ECG signal processing," *IEEE Trans. Biomed. Eng.*, vol. 55, no. 1, pp. 354–357, Jan. 2008.

[22] Q. Chen, G. Liu, and B. Han, "Suppression of imbalance vibration in AMB-rotor systems using adaptive frequency estimator," *IEEE Trans. Ind. Electron.*, vol. 62, no. 12, pp. 7696–7705, Dec. 2015.

[23] Y. Chen, M. Yang, J. Long, K. Hu, D. Xu, and F. Blaabjerg, "Analysis of oscillation frequency deviation in elastic coupling digital drive system and robust notch filter strategy," *IEEE Trans. Ind. Electron.*, vol. 66, no. 1, pp. 90–101, Jan. 2019.

[24] U. Nuss, "Blindleistungskompensation mit selbstgeführten stromrichter und kapazitivem energiespeicher," Ph.D. dissertation, Inst. Elect. Eng., Karlsruhe Inst. Technol., Karlsruhe, Germany, 1989.

[25] B. Burger and A. Engler, "Fast signal conditioning in single phase systems," in *Proc. Eur. Conf. Power Electron. Appl.*, 2001. [Online]. Available: http://www.epe-association.org/epe/index.php?main=/epe/documents.detail.php%3Fdocuments_id=2277

[26] J. Matas, H. Martin, J. de la Hoz, A. Abusorrah, Y. A. Al-Turki, and M. Al-Hindawi, "A family of gradient descent grid frequency estimators for the SOGI filter," *IEEE Trans. Power Electron.*, vol. 33, no. 7, pp. 5796–5810, Jul. 2018.

[27] M. Karimi-Ghartemani and A. Ziarani, "Performance characterization of a non-linear system as both an adaptive notch filter and a phase-locked loop," *Int. J. Adapt. Control Signal Process.*, vol. 18, no. 1, pp. 23–53, 2004.

[28] S. Golestan, J. M. Guerrero, and J. C. Vasquez, "Modeling and stability assessment of single-phase grid synchronization techniques: Linear time-periodic versus linear time-invariant frameworks," *IEEE Trans. Power Electron.*, vol. 34, no. 1, pp. 20–27, Jan. 2019.

[29] N. M. Wereley, "Analysis and control of linear periodically time varying systems," Ph.D. dissertation, Dept. Aeronaut. Astronaut., Massachusetts Inst. Technol., Cambridge, MA, USA, 1990.

[30] V. Salis, A. Costabeber, S. M. Cox, P. Zanchetta, and A. Formentini, "Stability boundary analysis in single-phase grid-connected inverters with PLL by LTP theory," *IEEE Trans. Power Electron.*, vol. 33, no. 5, pp. 4023–4036, May 2018.

[31] P. A. Regalia, "An improved lattice-based adaptive IIR notch filter," *IEEE Trans. Signal Process.*, vol. 39, no. 9, pp. 2124–2128, Sep. 1991.

[32] M. Bodson and S. C. Douglas, "Adaptive algorithms for the rejection of sinusoidal disturbances with unknown frequency," *Automatica*, vol. 33, no. 12, pp. 2213–2221, 1997.

[33] L. Hsu, R. Ortega, and G. Damm, "A globally convergent frequency estimator," *IEEE Trans. Autom. Control*, vol. 44, no. 4, pp. 698–713, Apr. 1999.

[34] M. Mojiri and A. Bakhshai, "An adaptive notch filter for frequency estimation of a periodic signal," *IEEE Trans. Autom. Control*, vol. 49, no. 2, pp. 314–318, Feb. 2004.

[35] Z. Xin, R. Zhao, P. Mattavelli, P. C. Loh, and F. Blaabjerg, "Re-investigation of generalized integrator based filters from a first-order-system perspective," *IEEE Access*, vol. 4, pp. 7131–7144, 2016.

[36] M. Karimi-Ghartemani, S. A. Khajehoddin, P. K. Jain, A. Bakhshai, and M. Mojiri, "Addressing dc component in PLL and notch filter algorithms," *IEEE Trans. Power Electron.*, vol. 27, no. 1, pp. 78–86, Jan. 2012.

[37] S. Golestan, J. M. Guerrero, and G. B. Gharehpetian, "Five approaches to deal with problem of dc offset in phase-locked loop algorithms: Design considerations and performance evaluations," *IEEE Trans. Power Electron.*, vol. 31, no. 1, pp. 648–661, Jan. 2016.

[38] M. Ciobotaru, R. Teodorescu, and V. G. Agelidis, "Offset rejection for PLL based synchronization in grid-connected converters," in *Proc. 23rd Annu. IEEE Appl. Power Electron. Conf. Expo.*, Feb. 2008, pp. 1611–1617.

[39] G. Fedele, A. Ferrise, and P. Muraca, "An adaptive quasi-notch filter for a biased sinusoidal signal estimation," in *Proc. 9th IEEE Int. Conf. Control Autom.*, Dec. 2011, pp. 1060–1065.

[40] J. Matas, M. Castilla, J. Miret, L. G. de Vicuna, and R. Guzman, "An adaptive prefiltering method to improve the speed/accuracy tradeoff of voltage sequence detection methods under adverse grid conditions," *IEEE Trans. Ind. Electron.*, vol. 61, no. 5, pp. 2139–2151, May 2014.

[41] Z. Xin, X. Wang, Z. Qin, M. Lu, P. C. Loh, and F. Blaabjerg, "An improved second-order generalized integrator based quadrature signal generator," *IEEE Trans. Power Electron.*, vol. 31, no. 12, pp. 8068–8073, Dec. 2016.

[42] M. Karimi-Ghartemani, S. A. Khajehoddin, P. K. Jain, and A. Bakhshai, "Problems of startup and phase jumps in PLL systems," *IEEE Trans. Power Electron.*, vol. 27, no. 4, pp. 1830–1838, Apr. 2012.

[43] J.-S. Park, T. H. Nguyen, and D.-C. Lee, "Advanced SOGI-FLL scheme based on fuzzy logic for single-phase grid-connected converters," *J. Power Electron.*, vol. 14, no. 3, pp. 598–607, May 2014.

[44] J. S. Park, D. C. Lee, and T. L. Van, "Advanced single-phase SOGI-FLL using self-tuning gain based on fuzzy logic," in *Proc. IEEE ECCE Asia Downunder*, Jun. 2013, pp. 1282–1288.

[45] H. Liu, Y. Xing, and H. Hu, "Enhanced frequency-locked loop with a comb filter under adverse grid conditions," *IEEE Trans. Power Electron.*, vol. 31, no. 12, pp. 8046–8051, Dec. 2016.

[46] H. A. Darwish and M. Fikri, "Practical considerations for recursive DFT implementation in numerical relays," *IEEE Trans. Power Del.*, vol. 22, no. 1, pp. 42–49, Jan. 2007.

[47] H. Ahmed, S. Amamra, and M. H. Bierhoff, "Frequency-locked loop based estimation of single-phase grid voltage parameters," *IEEE Trans. Ind. Electron.*, to be published.

[48] S. Golestan, J. M. Guerrero, J. C. Vasquez, A. M. Abusorrah, and Y. A. Al-Turki, "Single-phase FLLs based on linear Kalman filter, limit-cycle oscillator, and complex band-pass filter: Analysis and comparison with a standard FLL in grid applications," *IEEE Trans. Power Electron.*, to be published.

[49] K. Seifi and M. Moallem, "An adaptive PR controller for synchronizing grid-connected inverters," *IEEE Trans. Ind. Electron.*, vol. 66, no. 3, pp. 2034–2043, Mar. 2019.
[50] K. B. Ariyur and M. Krstic, *Real-Time Optimization by Extremum-Seeking Control*. Hoboken, NJ, USA: Wiley, 2003.
[51] C. A. Busada, H. G. Chiacchiarini, and J. C. Balda, "Synthesis of sinusoidal waveform references synchronized with periodic signals," *IEEE Trans. Power Electron.*, vol. 23, no. 2, pp. 581–590, Mar. 2008.
[52] M. S. Reza, M. Ciobotaru, and V. G. Agelidis, "Instantaneous power quality analysis using frequency adaptive Kalman filter technique," in *Proc. 7th Int. Power Electron. Motion Control Conf.*, Jun. 2012, vol. 1, pp. 81–87.
[53] M. S. Reza, M. Ciobotaru, and V. G. Agelidis, "Frequency adaptive linear Kalman filter for fast and accurate estimation of grid voltage parameters," in *Proc. IEEE Int. Conf. Power Syst. Technol.*, Oct. 2012, pp. 1–6.
[54] S. Reza, M. Ciobotaru, and V. G. Agelidis, "Accurate estimation of single-phase grid voltage fundamental amplitude and frequency by using a frequency adaptive linear Kalman filter," *IEEE J. Emerg. Sel. Topics Power Electron.*, vol. 4, no. 4, pp. 1226–1235, Dec. 2016.
[55] Z. Dai, Z. Zhang, Y. Yang, F. Blaabjerg, Y. Huangfu, and J. Zhang, "A fixed-length transfer delay based adaptive frequency-locked loop for single-phase systems," *IEEE Trans. Power Electron.*, vol. 34, no. 5, pp. 4000–4004, May 2019.
[56] P. Roncero-Sanchez, X. del Toro Garcia, A. P. Torres, and V. Feliu, "Robust frequency-estimation method for distorted and imbalanced three-phase systems using discrete filters," *IEEE Trans. Power Electron.*, vol. 26, no. 4, pp. 1089–1101, Apr. 2011.
[57] S. Golestan, J. M. Guerrero, and J. C. Vasquez, "An open-loop grid synchronization approach for single-phase applications," *IEEE Trans. Power Electron.*, vol. 33, no. 7, pp. 5548–5555, Jul. 2018.
[58] S. Golestan, J. M. Guerrero, A. Abusorrah, M. M. Al-Hindawi, and Y. Al-Turki, "An adaptive quadrature signal generation-based single-phase phase-locked loop for grid-connected applications," *IEEE Trans. Ind. Electron.*, vol. 64, no. 4, pp. 2848–2854, Apr. 2017.
[59] H. C. Lin, "Power harmonics and interharmonics measurement using recursive group-harmonic power minimizing algorithm," *IEEE Trans. Ind. Electron.*, vol. 59, no. 2, pp. 1184–1193, Feb. 2012.
[60] M. Mojiri, M. Karimi-Ghartemani, and A. Bakhshai, "Processing of harmonics and interharmonics using an adaptive notch filter," *IEEE Trans. Power Del.*, vol. 25, no. 2, pp. 534–542, Apr. 2010.
[61] H. Zamani, M. Karimi-Ghartemani, and M. Mojiri, "Analysis of power system oscillations from PMU data using an EPLL-based approach," *IEEE Trans. Instrum. Meas.*, vol. 67, no. 2, pp. 307–316, Feb. 2018.
[62] C. Chen, J. Xiong, Z. Wan, J. Lei, and K. Zhang, "A time delay compensation method based on area equivalence for active damping of an LCL-type converter," *IEEE Trans. Power Electron.*, vol. 32, no. 1, pp. 762–772, Jan. 2017.
[63] Q. Yan, R. Zhao, X. Yuan, W. Ma, and J. He, "A DSOGI-FLL-based dead-time elimination PWM for three-phase power converters," *IEEE Trans. Power Electron.*, vol. 34, no. 3, pp. 2805–2818, Mar. 2019.
[64] Z. Xin, P. C. Loh, X. Wang, F. Blaabjerg, and Y. Tang, "Highly accurate derivatives for LCL-filtered grid converter with capacitor voltage active damping," *IEEE Trans. Power Electron.*, vol. 31, no. 5, pp. 3612–3625, May 2016.
[65] Z. Xin, R. Zhao, X. Wang, P. C. Loh, and F. Blaabjerg, "Four new applications of second-order generalized integrator quadrature signal generator," in *Proc. IEEE Appl. Power Electron. Conf. Expo.*, Mar. 2016, pp. 2207–2214.
[66] M. Castilla, J. Miret, J. Matas, L. G. de Vicuna, and J. M. Guerrero, "Control design guidelines for single-phase grid-connected photovoltaic inverters with damped resonant harmonic compensators," *IEEE Trans. Ind. Electron.*, vol. 56, no. 11, pp. 4492–4501, Nov. 2009.
[67] M. Castilla, J. Miret, J. Matas, L. G. de Vicuna, and J. M. Guerrero, "Linear current control scheme with series resonant harmonic compensator for single-phase grid-connected photovoltaic inverters," *IEEE Trans. Ind. Electron.*, vol. 55, no. 7, pp. 2724–2733, Jul. 2008.
[68] M. Karimi-Ghartemani, "Linear and pseudolinear enhanced phased-locked loop (EPLL) structures," *IEEE Trans. Ind. Electron.*, vol. 61, no. 3, pp. 1464–1474, Mar. 2014.
[69] M. Karimi-Ghartemani, "A unifying approach to single-phase synchronous reference frame PLLs," *IEEE Trans. Power Electron.*, vol. 28, no. 10, pp. 4550–4556, Oct. 2013.
[70] M. Mojiri, M. Karimi-Ghartemani, and A. Bakhshai, "Estimation of power system frequency using an adaptive notch filter," *IEEE Trans. Instrum. Meas.*, vol. 56, no. 6, pp. 2470–2477, Dec. 2007.
[71] S. A. Khajehoddin, M. Karimi-Ghartemani, P. K. Jain, and A. Bakhshai, "A resonant controller with high structural robustness for fixed-point digital implementations," *IEEE Trans. Power Electron.*, vol. 27, no. 7, pp. 3352–3362, Jul. 2012.
[72] M. Ciobotaru, R. Teodorescu, and F. Blaabjerg, "A new single-phase PLL structure based on second order generalized integrator," in *Proc. 37th IEEE Power Electron. Spec. Conf.*, Jun. 2006, pp. 1–6.
[73] C. Yang, J. Wang, X. You, C. Wang, and M. Zhou, "Comparison of discretization methods on the second-order generalized integrator frequency-locked loop," in *Proc. IEEE Energy Convers. Congr. Expo.*, Sep. 2018, pp. 3095–3102.
[74] F. Tedesco, A. Casavola, and G. Fedele, "Unbiased estimation of sinusoidal signal parameters via discrete-time frequency-locked-loop filters," *IEEE Trans. Autom. Control*, vol. 62, no. 3, pp. 1484–1490, Mar. 2017.
[75] F. J. Rodriguez, E. Bueno, M. Aredes, L. G. B. Rolim, F. A. S. Neves, and M. C. Cavalcanti, "Discrete-time implementation of second order generalized integrators for grid converters," in *Proc. 34th Annu. Conf. IEEE Ind. Electron. Soc.*, Nov. 2008, pp. 176–181.

Authors' photographs and biographies not available at the time of publication.